Developing luminescence analysis of Icelandic volcanic glass: a case study using the Þórsmörk Ignimbrite

Stephen J. Roberts[1, *], David C.W. Sanderson[2], Andrew J. Dugmore[3]

[1] British Antarctic Survey (BAS), Natural Environment Research Council (NERC), High Cross, Madingley Rd, Cambridge, CB3 0ET, UK.

[2] SUERC, Scottish Enterprise Technology Park, Rankine Avenue, East Kilbride, Glasgow G75 OQF, Scotland.

[3] School of GeoSciences, University of Edinburgh, Drummond Street, Edinburgh EH8 9XP.

***Corresponding author:**

e-mail: sjro@bas.ac.uk, Tel: +44 (0)1223 221 339; Fax: +44 (0)1223 221 259

Twitte: @roberts_sjr

This paper is a non-peer reviewed preprint submitted to EarthArXiv

Keywords: Tephra; geochronology; geochemistry; Arctic; palaeoclimate

Abstract

Large volcanic eruptions from Iceland can produce significant volumes of glass-rich rhyolitic tephra, which are then deposited across NW Europe and the North Atlantic-Arctic region, forming time-parallel marker horizons useful to palaeoenvironmental studies. Here we investigate new ways of improving the tephrochronological record of Iceland using (thermo)luminescence analysis of rhyolitic volcanic glass shards that dominate airfall ash deposits of the Þórsmörk Ignimbrite (ÞIG), tephra from the Askja 1875 AD, Öræfi 1362 AD eruptions, and the Óþoli tephra from NW Iceland. Following screening experiments, which showed that pure volcanic glass samples retained age-related TL signals, we undertook glass-phase TL dating of the ÞIG and Óþoli tephra. Our TL age estimate of c. 40 ± 10 ka for the ÞIG supports phenocryst-based radiometric ages of c. 50 ka rather than older age estimates of c. 200 ka. Results from the Óþoli tephra were consistent with the fission track age established at c. 2 Ma age, but further investigations of high dose sensitivity changes and longer-term stability factors such as athermal fading are required for quantitative dating of volcanic glass deposits >100 ka. However, as thermoluminescence signals from purified glass fractions of Icelandic tephra can be obtained over 100–1,000,000-year time scales, luminescence characterisation of glass shards can be used alongside geochemical and morphological analysis to distinguish between distal tephras with similar geochemical signatures, and assist with tephrochronological investigations beyond the limits of radiocarbon dating.

Introduction

Large explosive rhyolite-producing eruptions from Iceland, such as the one responsible for the Þórsmörk Ignimbrite (ÞIG) in southern Iceland (Fig. 1), are comparatively rare, but particularly useful as they form time-parallel marker horizon, which provide chronological constraints for palaeoenvironmental records. As recent eruptions from Iceland have shown, volcanic ash from even comparatively small eruptions can be distributed across the North Atlantic and Arctic regions, and north-western Europe. Numerous studies have used of tephra layers to link ice, marine and terrestrial records of past environmental and climate change [1–30], but glacial erosion has removed many of the largest eruptions of the pre-Holocene, Quaternary era (>11.7 ka–2.5 Ma) from the Icelandic terrestrial record and some key large Pleistocene eruptions remain relatively poorly characterised and dated near their sources.

To be useful as time-parallel marker horizons, tephra deposits need to be fully characterised. Major and trace element geochemistry and phenocrystic composition are commonly used alongside shard morphology, texture and chronological data to distinguish between different tephra deposits, and correlate those that are similar [24, 27–42]. However, geochemical correlation based on glass major element geochemistry can sometimes be problematic. Multiple eruptions from the same magma body can produce geochemical heterogeneity within the glassy products of individual deposits [43, 44], but different eruptions from the same magma chamber over a period of time can also produce glass with broadly similar major element geochemical composition. Recent studies have shown there are significantly more visible and non-visible (crypto-tephra) Icelandic ash deposits in sediment cores extracted from the Arctic Sea and North Atlantic than previously thought, and not all can be distinguished by shard-specific major or trace element analysis [33, 37]. Widely dispersed

tephra deposits can also be re-deposited a long time after the eruption event by post eruption processes such as ice-rafting [45, 46] and several studies have confirmed that glass is not geochemically stable in all burial environments or able to withstand harsh laboratory digestion procedures intact [47, 48].

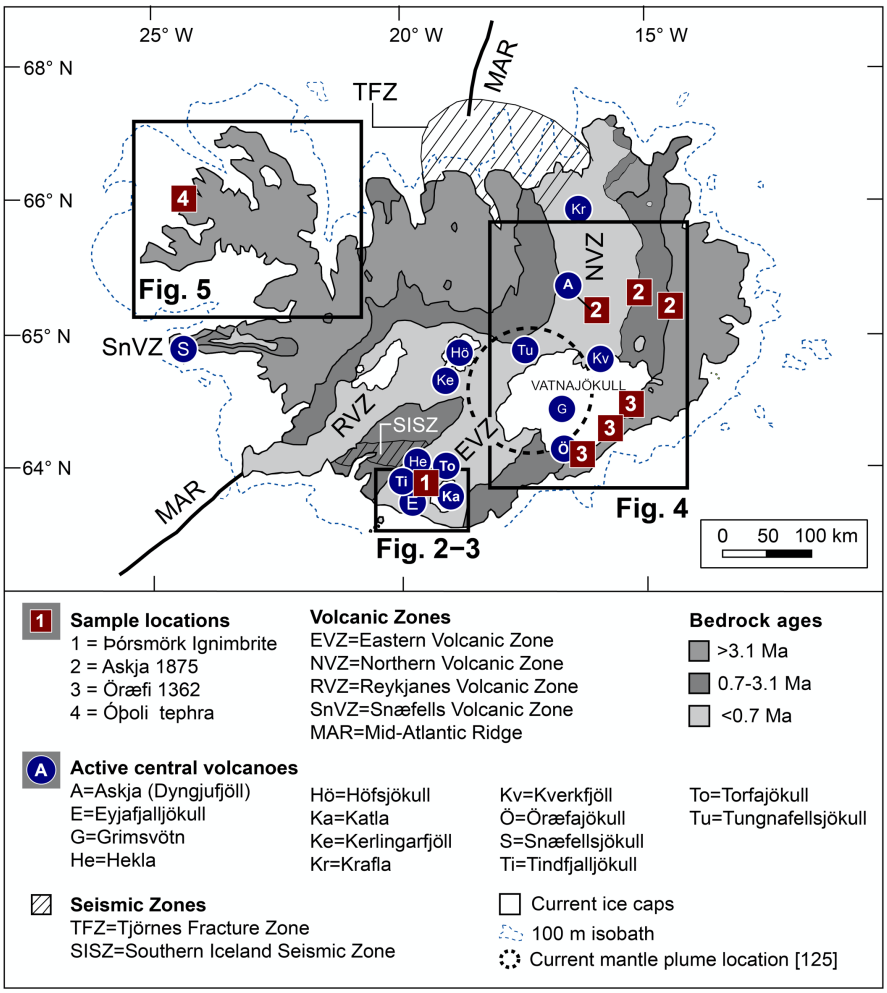

Figure 1. Summary geological map of Iceland showing active central volcanoes and sample locations [adapted from 11].

More than 300 historical eruptions have been documented or identified by geochemical analysis of tephra layers in Iceland in the last c. 1,100 years, on average, one every four years [7, 10, 11, 29, 49-59]. Tephra is the only product of more than 130 of these eruptions, and

74 over 75 % of these have produced a visible tephra layer on the Icelandic mainland [60].
75 However, rhyolitic tephra and large ignimbrite-forming eruptions are relatively uncommon in
76 the Icelandic tephrochronological record [13, 15, 37, 53, 61].
77
78 Since rhyolitic magmas produce the most geochemically evolved and distinctive tephra,
79 geochemical discrimination between different volcanic systems and/or multiple eruption
80 events from the same volcanic system can be achieved. Moreover, large volumes of rhyolitic
81 volcanic glass, which are unequivocally associated with the eruption event, form explosively
82 on contact with water and/or ice during magma-quenching. For example, volcanic glass
83 formed from the rhyolitic magma of the Öræfi 1362 AD eruption is geochemically
84 homogenous and has <1% phenocrystic content [62]. Glass-rich volcanic ash ejected into the
85 stratosphere can be distributed over a wide geographical area, forming long-distance
86 chronological markers [63, 64]. Advantageously, selective removal of heavier phenocrystic
87 components during long-distance stratospheric transport of ash provides a natural glass-
88 purification process.
89
90 Radiation induced thermoluminescence (TL) is a well-established property of crystalline
91 minerals such as quartz and feldspars [65]. Non-crystalline materials including synthetic glass
92 [66,67] and naturally occurring volcanic glass (*e.g.*, obsidian) [68] also exhibit TL, though with
93 lower sensitivities than most crystalline materials. A study of 55 archeaological silicate glass
94 slices [66] showed high temperature TL sensitivities ranging from 10^{-1} to 10^{2} photon counts
95 per mg per Gy in 10 degree centrigrade bands. By contrast TL sensitivities from quartz samples
96 from diverse lithologies have been reported [111] as ranging from 10^{3}-$2x10^{4}$ photon counts

per mg per Gy over similar temperature intervals (centred on 380 degrees centigrade), and from feldspars from 10^4-10^6 phioton counts per mg per Gy.

Therefore, though volcanic glass is a metastable material [72], luminescence signals from the glass phase of tephra provide a useful additional provenance and, potentially, chronological tool, especially in the c. 50-75 ka age-range, which is difficult to date radiometrically in the absence of suitable phenocrysts [68–70]. Despite the relatively low signal levels, and variability in signal outputs due to retention of some fine crystalline components, pioneering luminescence studies from the early 1980s on fine-grained volcanic glass-rich fractions from tephra deposits from North America and New Zealand showed considerable potential [73–74].

Here, first, we investigate new ways of improving the tephrochronological record of Iceland bycharacterising the geochemical and TL properties of the (airfall) rhyolitic glass component that dominates tephra (>95%) from four key rhyolitic Icelandic eruptions of Late Quaternary age: the Þórsmörk Ignimbrite (ÞIG), the Óþoli tephra (ÓT), the Askja 1875 AD (A1875) and Öræfi 1362 AD (Ö1362) eruptions and (Figs. 1–6; Supplementary Fig. S1, Table S1). Second, we focus on producing quantitative ages from the ÞIG and compare our results to published age estimates.

Based on geochemical correlation to potassium-argon dated phenocrysts from ignimbrite deposits outside of the Þórsmörk area [1, 2], the ÞIG was originally considered to be c. 200 ka. An argon-argon (Ar-Ar) age of 54.5 ± 2 ka [3] has been geochemically linked to the c. 55 ka North Atlantic Ash Zone-II (NAAZ-II) II-RHY-II deposit, a widespread and geochemically

121 homogenous tephra deposit found in North Atlantic and Arctic Sea marine sediment cores
122 Greenland ice core records [3–5]. The eruption that formed the ÞIG is the same order of
123 magnitude as the thickest rhyolitic tephra layers in the Holocene and historical
124 tephrochronological record of Iceland, *e.g.*, Hekla 3, Hekla 4, Öræfi 1362 AD and Askja 1875
125 AD [11, 76, 88, 89].
126
127 The Óþoli tephra was found in plateau-top ice-dammed lake deposits of NW Iceland.
128 Following initial TL analysis which suggested an early Quaternary age and has been fission-
129 track dated to 2.26 ± 0.11 Ma [75]. In this study, the tephra deposit acts as an 'older' age-
130 comparison for quantitative TL dating of purified volcanic glass from the ÞIG.
131
132 The A1875 and Ö1362 tephra deposits examined are from two of the largest rhyolite forming
133 Plinian eruptions in the Icelandic historical record. These eruptions distributed large volumes
134 of tephra across eastern Iceland and NW Europe. In this study, we use them as 'recent' TL
135 age-controls because they have similar glass-phase rhyolitic geochemistry to the Óþoli tephra
136 and the ÞIG.
137
138 **Study sites**
139
140 ***Þórsmörk Ignimbrite****:* The Þórsmörk Ignimbrite (ÞIG), first described by Thórarinsson [1] and
141 named by Jørgensen [76, 77], is located in the transitional-alkalic province of the Eastern
142 Volcanic Zone (Fig. 1). It is one of Iceland's largest eruptive bodies, covering an area of about
143 80 km^2 (Figs. 2, 3). Outcrops in the Þórsmörk area are the only known record of the ÞIG-
144 forming eruption in the Icelandic terrestrial tephra record. Intermittent volcanic aggradation

and glacial erosion have exposed well-preserved stratigraphic sections along the Krossa and Markarfljót valleys, with deposits north of the Krossa that are typically 10–50 m thick but can be up to 200 m thick [76, 77] (Figs. 2, 3). Accessible exposures, up to 30 m thick, are located on a 4–5 km stretch along the northern border of the Krossa (Figs. 2, 3). No basal contact is visible at most sites and only slope deposits are accessible at some sites [1, 76] (Fig. 3).

The Þórsmörk area is surrounded by three ice-capped, active central volcanoes: Eyjafjalljökull to the south, Katla to the east, Tindfjalljökull to the north (Fig. 2b). Torfajökull, Iceland's largest active rhyolite volcano, is located further to the NE and Hekla is located further north beyond Tindfjalljökull. Torfajökull is amongst the most active rhyolitic volcanoes in the world with at least ten rhyolitic eruptions in the post-glacial period alone with the last occurring in ca. 1480 AD [78]. Tindfjalljökull is the least active central volcano in this region and classified as a dormant volcano because there have only been a few eruptions along its margins in post-glacial times [1, 79, 80]. Eruptions from Tindfjalljökull are typically dominated by slightly alkaline basalts and minor intermediate rocks and abundant sub-alkaline to slightly peralkaline rhyolites [76, 80–83]. Thórarinsson suggested that the summit of Tindfjalljökull is collapse caldera connected with the formation of the ÞIG [1, 76, 84]. All structural and depositional features of the ÞIG preserved in and around Þórsmörk are associated with emplacement from pyroclastic flows or surges [76, 77] (Fig. 3). Jørgensen [76, 77] found no evidence for a Plinian phase of activity, but abundant airfall ash deposits (*e.g.*, Fig. 3i–l) could have been formed by explosively-generated pyroclastic flows, created by instabilities in the lower parts of the eruption column [85]. These combined into an ignimbrite-forming surge that mantled the existing topography, with welded and unwelded pumice and ash forced into valley troughs and sides. Given an average thickness of 20-25 m, Thórarinsson [1] calculated

169 that the equivalent volume of the ÞIG as 1.5–2.0 km^3. At least a further 2–3 km^3 of freshly
170 fallen tephra was probably dispersed over a wider area, but this has since been eroded by
171 glacial activity.

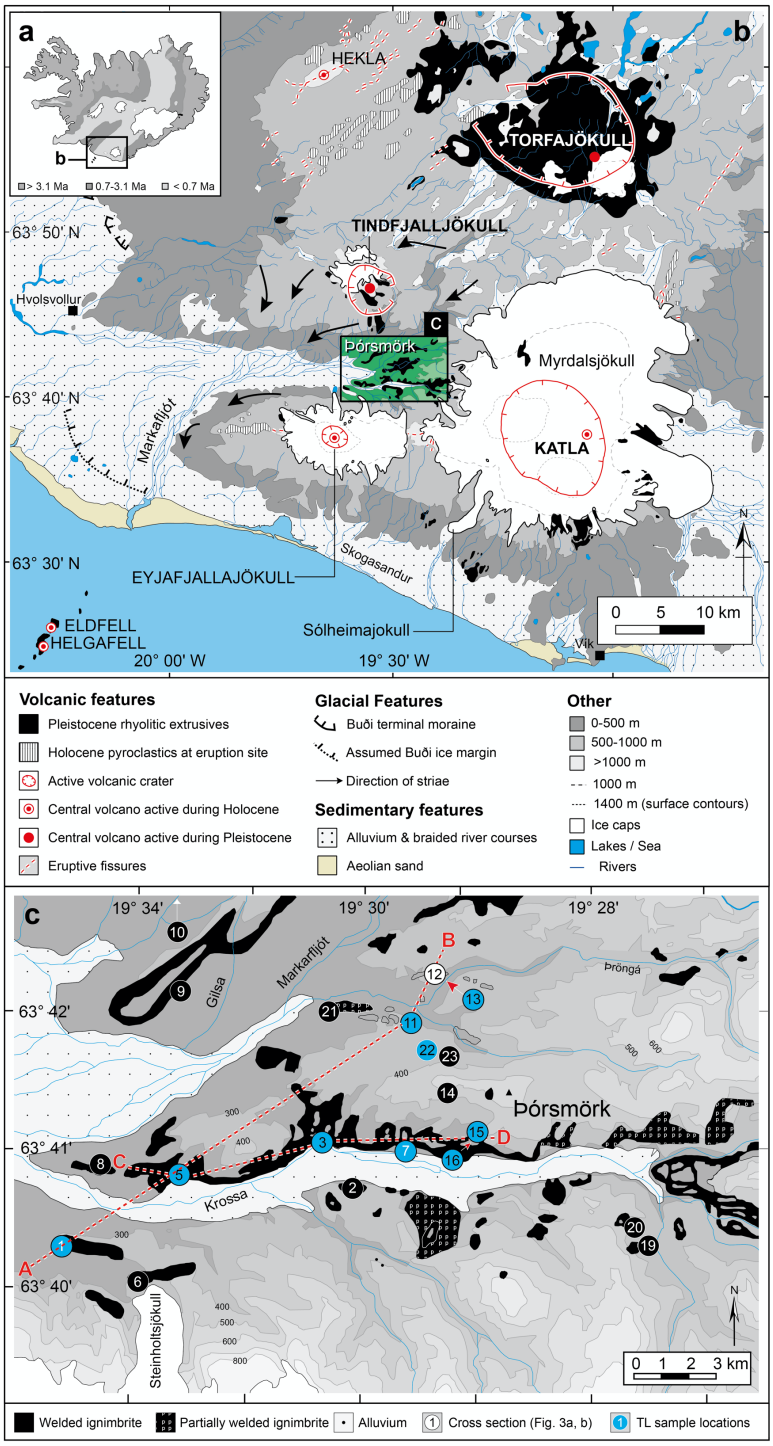

172

173 **Figure 2. Regional setting and sampling locations for the Þórsmörk Ignimbrite. (a)** Location
174 map of Iceland; **(b)** Location map of Þórsmörk in relation to active volcanoes, pyroclastic and

extrusive deposits and main glacial features of the Eastern Volcanic Zone (EVZ), Iceland. The geology of area covered by the Þórsmörk box is basic and intermediate hyaloclastites and tuffaceous sediment younger than 0.7 Ma (based on the 1:250,000 Geological Map no. 6 of the Iceland Geodetic Survey). **(c)** Sketch map of main outcrops of the Þórsmörk Ignimbrite, and its broad classification into welded and unwelded outcrops [adapted from 76, 77] and thermoluminescence sampling locations (blue circles) investigated in this study. Some sample sites (*e.g.*, ÞIG10) were located off-map, while others (*e.g.*, ÞIG12) were inaccessible.

Thórarinsson [1] and Jørgensen [77] both suggested a c. 200 ka age for the ÞIG by correlating deposits in Þórsmörk with potassium-argon (K-Ar) ages from geochemically similar deposits north of Þórsmörk [2, 4]. Zielinski et al. [9] later proposed that the ÞIG was the source of the rhyolitic component of North Atlantic Ash Zone-II (NAAZ-II), a widespread tephra deposit that has been found in numerous marine and ice cores across the North Atlantic and the Arctic Sea (Fig. S1). Dated to c. 50 ka, based on its correlation-based age in the GISP2 Greenland ice core of 53.5-55 ka [9, 86, 87], NAAZII has been geochemically linked with an argon-argon (Ar-Ar) dated ÞIG deposit of 54.5 ± 2.0 ka, sampled from an unspecified location [3].

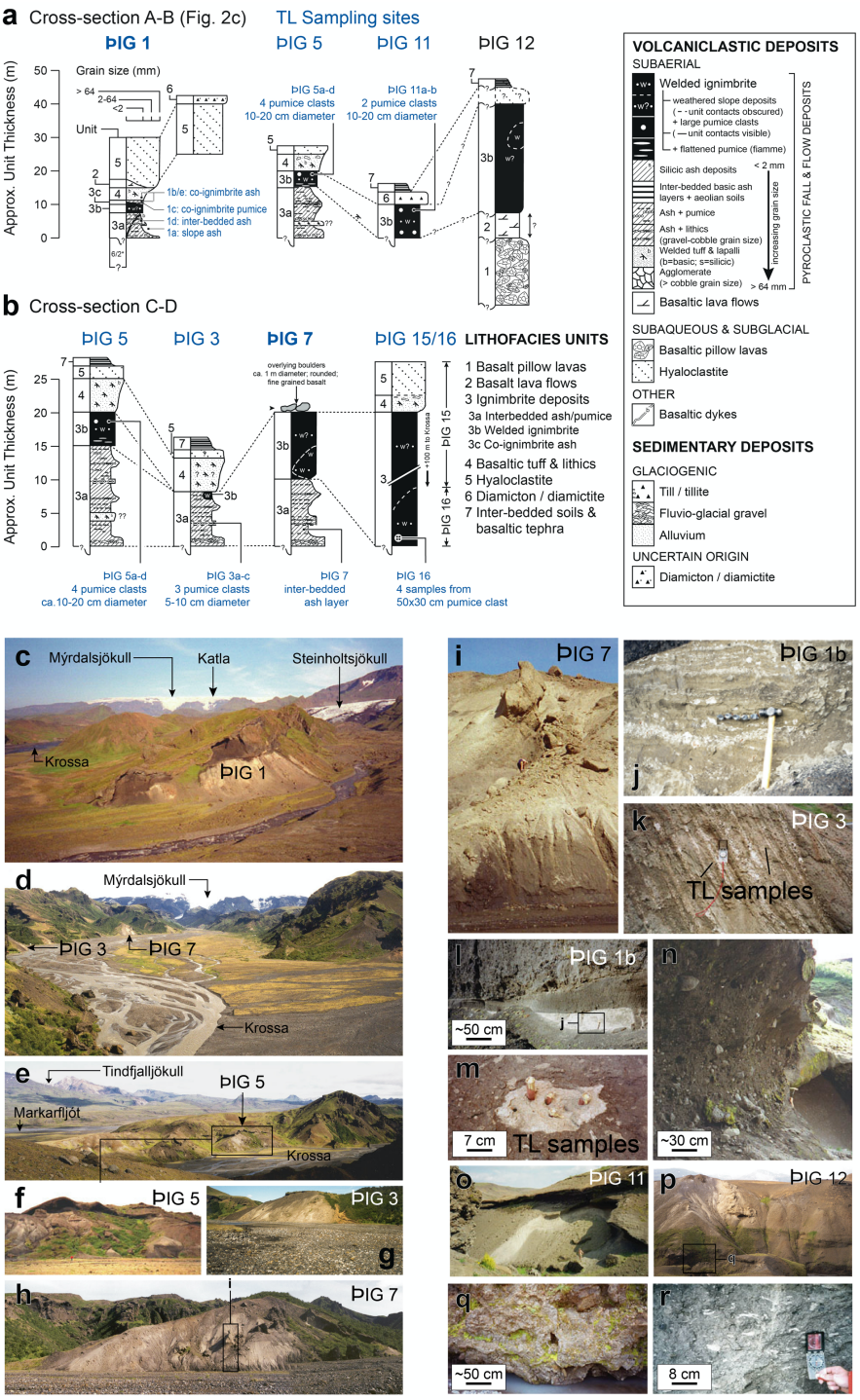

191

192 **Figure 3. The Þórsmörk Ignimbrite, southern Iceland. (a–b)** Summary composite schematic
193 stratigraphic logs of main lithofacies units at principal sites and schematic cross section
194 sketches along lines A-B and C-D; **(c–r)** Photographs of the Þórsmörk Ignimbrite sampling
195 locations and luminescence sampling methods: **(c)** Site ÞIG 1, taken from the lateral moraine
196 of Gigjökull, looking approximately E up the Krossa towards Mýrdalsjökull; **(d)** Sites ÞIG 3 & 7,

taken from Valahnjúkur looking approximately E up the Krossa towards Mýrdalsjökull; **(e)** Site ÞIG 5, taken from the top of site ÞIG 6, looking approximately NNE towards Tindfjalljökull in the distance; **(f)** Site ÞIG 5; **(g)** Site ÞIG 3 looking approximately W down the Krossa; **(h)** Site ÞIG 7 taken from the Krossa sandur looking N at sampling site, and erratics near the top of the deposit (circled); **(i)** TL sampling at site ÞIG 7 composed of inter-bedded ash, pumice and lithic layers beneath an outcrop of welded ignimbrite, similar to those at ÞIG 3, shown in (k); **(j)** TL sampling at ÞIG 1b in ash rich co-ignimbrite ash and pumice layers; **(k)** TL sampling of inter-bedded ash layers at ÞIG 3; **(l)** Co-ignimbrite ash, black tuff and capping hyaloclastites at site ÞIG 1b (Units 3c, 4, 5); **(m)** TL sampling of a large pumice clast, c. 25–30 cm in diameter, embedded in a welded ash and lithic matrix at site ÞIG 16; **(n)** Poorly sorted, rounded boulders and pebbles in loose soil and fine-grained matrix (diamicton) contact with welded ignimbrite at site ÞIG 11 (hammer for scale); **(o)** Site ÞIG 11 looking NNE (person at the bottom edge of the shadow for scale); **(p)** Site ÞIG 12 taken from the top of the hill at site ÞIG 13 looking approximately north; **(q)** Pillow lavas at the base of ÞIG 12; **(r)** Fiamme at the base of ÞIG 5 (Unit 3b).

Askja 1875 AD (A1875) tephra: Post-glacial volcanism in Iceland is concentrated in four separate areas within the fissure system of Dyngjufjöll (Askja), located approximately 100 km North of Vatnajökull in the Eastern Highlands of the tholeiitic Northern Volcanic Zone (NVZ) of Iceland (Figs. 1, 4) [83]. Askja, the name of the main caldera and central volcano, covers an area of c. 45 km^2 (Fig. 4) and is bounded by steep cliffs, with Pleistocene-age rocks and predominantly basaltic composition forming the basement bedrock inside the crater (Fig. 4) [89]. Post-glacial lavas contain several rhyolitic ash layers, the oldest dated to c. 9,800 years BP [90]. Between 9,800-4,500 years BP, following rapid early Holocene deglaciation in Iceland,

volcanic productivity was 30 times greater than during the historical era [90]. The last Plinian eruption in the Dyngjufjöll volcano took place from within the Askja caldera a few hours before 8 a.m. on 29th March 1875 AD [90, 91]. The explosive phase of the eruption produced large volumes of fine-grained, grey-white, non-vesicular ash, which was dispersed across eastern Iceland by strong westerly winds forming visible layers 20-30 cm thick up to 50 km away [6]. The A1875 eruption is a classic example of how tephra from explosive Icelandic eruptions can be rapidly distributed across the North Atlantic and NW Europe [92, 93]. Tephra layers dominated by glass-shards invisible to the naked eye with a similar eruption-related geochemistry to A1875 deposits in Iceland have been found in Scandinavia [90, 94].

Öræfi AD1362: The Öræfajökull volcano, located in the Eastern Volcanic Zone on the southern margins of the Vatnajökull ice cap (Figs. 1, 4b), is Iceland's highest (2119 m) and most active composite stratovolcano during the post-glacial and Holocene era. There have only been two rhyolite-producing eruptions from Öræfajökull in the historical period: in 1362 AD and 1727 AD [11]. The 1362 AD eruption (henceforth referred to as Ö1362) was particularly explosive, producing >10 km^3 of freshly fallen rhyolitc ash and pumice, and accompanied by two massive jökulhlaups from Falljökull and Rótarfjallsjökull. Although the eruption took place mainly in the caldera, and most of the fallout occurred over the sea, it is still the second most voluminous tephra deposit in Iceland in recorded history, after the more effusive and basaltic tephra producing Veiðivötn eruption of 1477 AD [58]. Up to 2 km^3 of highly evolved rhyolitic (SiO_2>70%) tephra fell on land with prevailing westerly winds transporting most of the ejecta ESE across the North Atlantic [11, 62, 95]. Tephra layers up to 10 cm thick have been found in soils covering an area of 4300 km^2 surrounding the main edifice [96].

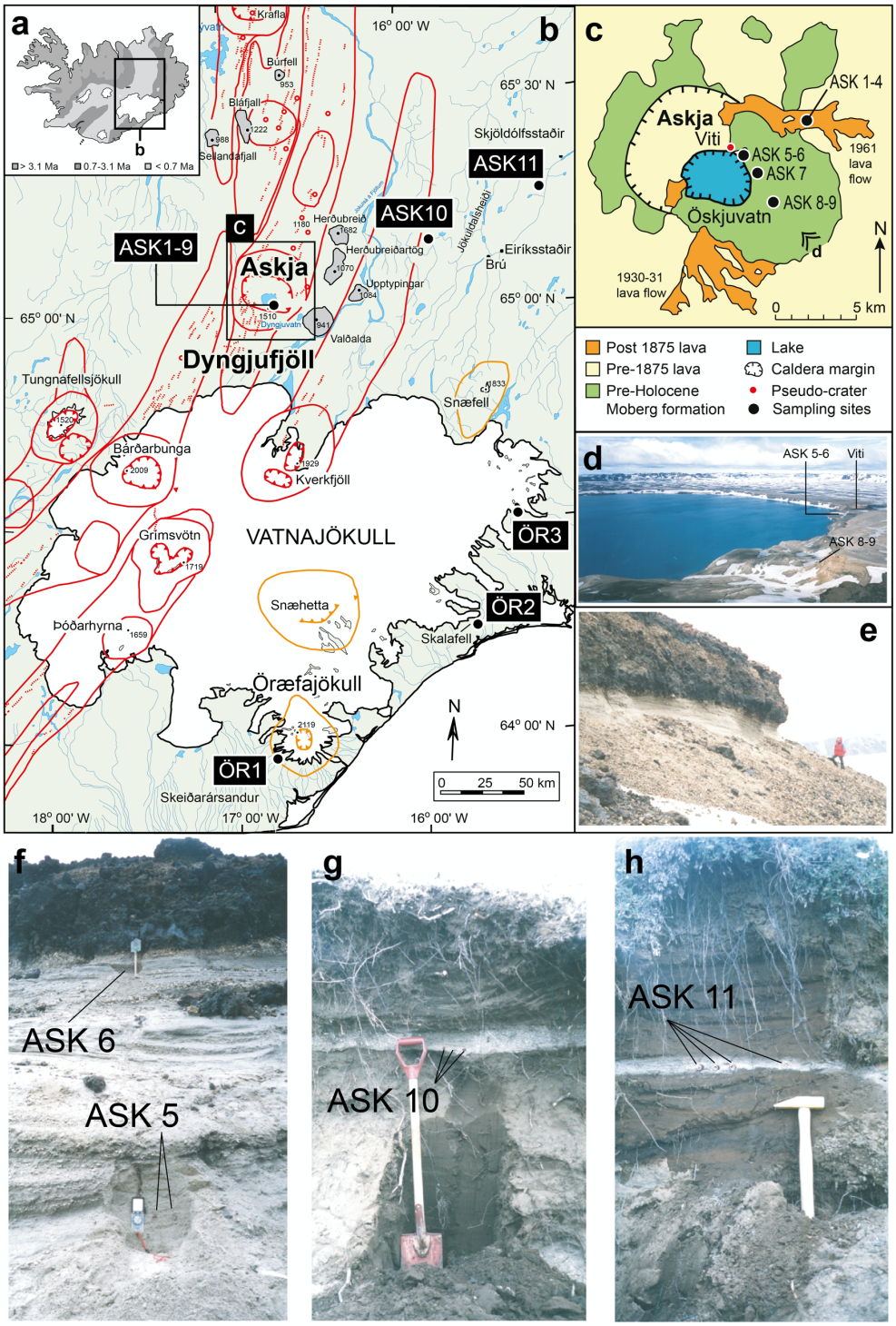

Figure 4. Historical eruption age-control study sites and sampling of A1875 and Ö1362 tephra deposits. (a) Location map; **(b)** Regional setting of the Askja (Dyngjufjöll) (red) and the Öræfi (orange) volcanic systems and Askja 1875 (ASK1-11) and Öræfi 1362 (ÖR1-3) sampling locations. Solid red & orange lines are outlines of the main volcanic systems; broken lines red and orange lines are fissure swarms; triangulated lines are the caldera margin; red circles are

craters and grey areas outlines of the main table mountains ('mobergs'). **(c)** Summary geological map of Askja adapted from [89] and showing the location of samples ASK 1-9. **(d)** Askja caldera from SE rim and ASK 5-9 sampling sites; **(e)** A1875, Layer 'D' [89] and capping lava flow; **(f)** TL sampling of Askja 1875 - ASK 5 (Layer 'C' [89] and ASK 6 (Layer 'D' [89]); **(g)** ASK 10 at Fiskidalur, 55 km NNE of Askja; **(h)** ASK 11 at Arnórsstaðamuli, 74 km NNE of Askja.

Óþoli Tephra: The Óþoli tephra (ÓT) is a rhyolitic tephra deposit within a glacio-lacustrine sedimentary sequence near the plateau surface of Skagafjall [75, 97] (Fig. 5a–c). The ÓT sedimentary unit consists of 8-10 cm of airfall tephra overlain by up to c. 10 m of reworked volcanic ash (Fig. 5d). The airfall ash sub-unit is composed of more than 99% rhyolitic glass, with very minor basaltic–andesite/andesitic altered glass and sparse traces of feldspar, iron ore and pyroxene of uncertain origin [75, 97]. The 8–10 cm thick airfall ash is unusual for a tephra deposit on the NW (Vestfírðir) Peninsula, where visible tephra layers in Holocene peat deposits are uncommon, and usually less than a centimetre thick (Fig. 5d). Based on its stratigraphic position within an ice-dammed lake sequence in NW Iceland, the ÓT was originally thought to have been deposited c. 17–23 ka [97], but has since been dated to 2.26 ± 0.11 Ma using the isothermal fission-track method [75]. Prior to fission-track dating analysis, preliminary luminescence experiments on the airfall rhyolitic glass fraction revealed the ÓT had a minimum age of at least c. 400 ka (Fig. 6f) [75]. The ÓT is most likely the product of a large Plinian-style eruption somewhere in the Húsafell region, a now inactive part of the SW Iceland axial rift (RVZ in Fig. 1) from near-central Iceland [75]. Prevailing north/north-north-westerly winds at the time of the eruption transported ash c. 200 km, depositing it on the heavily glaciated landscape of the Vestfírðir Peninsula during the Late Pliocene [75]. The A1875 tephra is the closest geochemical match to the Óþoli tephra (Figs. 1, S1) [75].

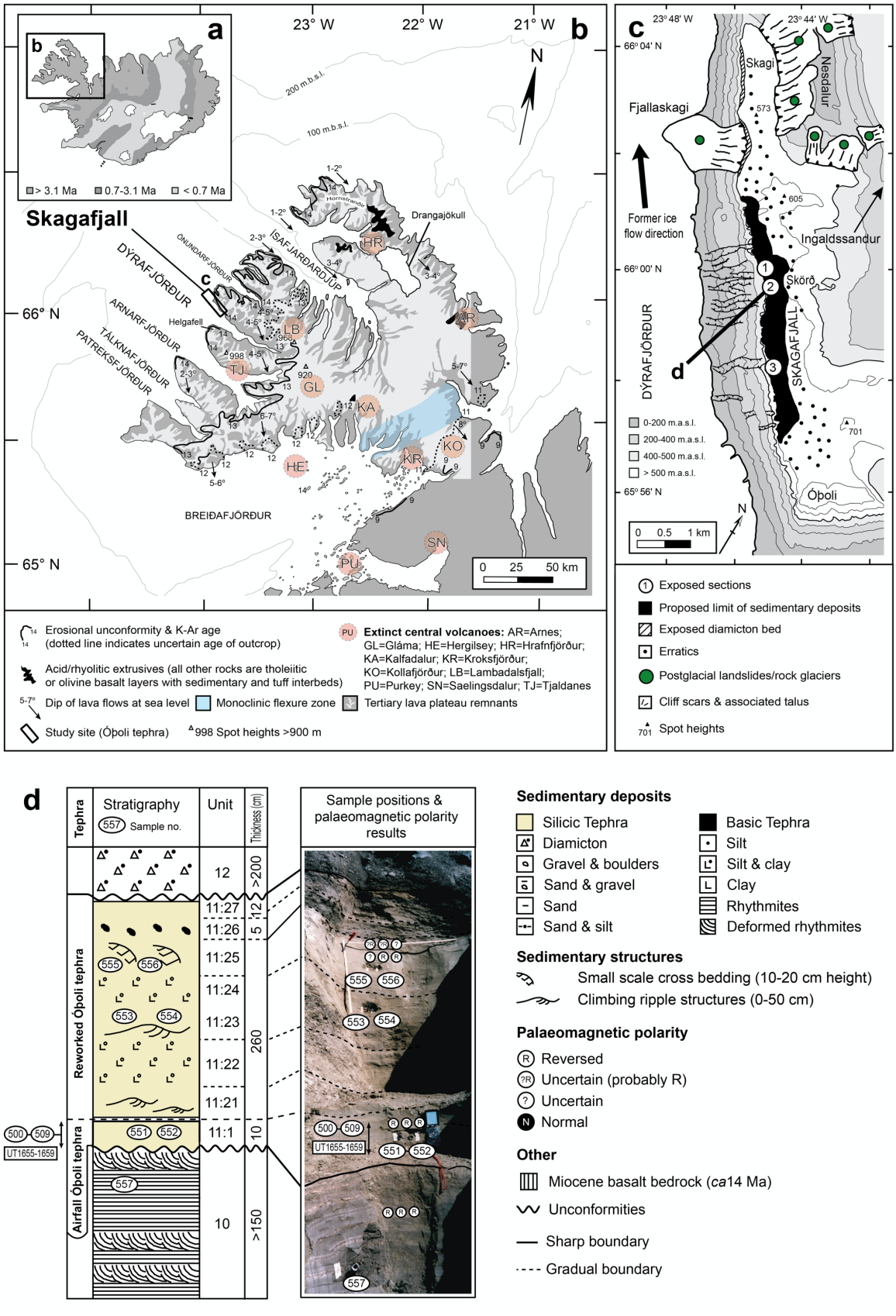

Figure 5. Regional setting, stratigraphic logs and sampling of the Óþoli tephra. (a–c) Location of Skagafjall and main geological features of the Western Troughs of the Vestfirðir Peninsula

(based on [75, 97]). **(d)** Detailed stratigraphic log of and summary of palaeomagnetic results from Skagafjall section B units 10–12 and sampling strategy/sample numbers for the air fall and reworked components of the Óþoli tephra. Sample numbers 500-510 and 551-557 are SUTL laboratory numbers (SUERC-luminescence dating laboratory) sampled from the airfall tephra deposits in section B. SUTL558 is from section C. SUTL500-509 were sampled at 1 cm intervals from the basal 10 cm of Óþoli tephra above the rhythmite bed/tephra contact; UT sample numbers are University of Toronto fission-track laboratory numbers [97].

Methods

Luminescence dating relies on the laboratory reconstruction of the radiation dose absorbed by sensitive materials in the natural environment since formation or since the last heat- or light- induced resetting or 'zeroing' event [98–100]. For volcanic glass, the event being dated is the formation event, *i.e.*, cooling from magma, which due to its extremely high temperature, may be assumed to be free from residual thermoluminescence signals. Here, this assumption was verified, for practical purposes, using 19th Century material from the A1875 eruption. A laboratory determination of the total radiation dose experienced since the formation or last bleaching event is referred to as the equivalent or palaeodose, D_e. This is obtained, following measurement of the "natural" luminescence signal in the laboratory by reconstructing a stepwise luminescence dose-response curve by laboratory irradiation, and remeasurement of stimulated luminescence from purified sub-samples (or aliquot discs). If D_T , the rate of radiation dose received by decay of radioactive elements, and cosmic radiation, *in-situ* in the natural environment, can be reliably assessed [99, 100], an age estimate can be determined, simply, as the quotient of palaeodose (D_e) and environmental dose rate (D_T) or [D_e / D_T].

Sample collection and purification

We examined the luminescence characteristics of undisturbed airfall deposits to avoid possible complications associated with post-depositional reworking and light exposure. Samples were collected by hammering light tight 22–27 mm diameter, 20–50 cm long copper tubes into airfall tephra and pumice deposits that had been cut back 10–30 cm. All samples were transported and stored under light-tight conditions and 2–5 cm of material at the end of the tubes that could have been exposed to light was removed.

Contaminant mineral phases that also retain a luminescence signal, such as quartz, feldspar and zircon, have a higher density (>2.45 g cm^{-3}) than rhyolitic glass (2–2.2 g cm^{-3}). Therefore, double-purified sieved 90–150 μm volcanic glass fractions were prepared by density separation techniques [48, 73, 102]. Samples were cleaned ultrasonically in 10% hydrochloric acid (HCl) and density separated 2.3–2.4 or <2.4 g cm^{-3} using sodium polytungstate solution (Figs. S1, S3). Harsh chemical treatments and etching were avoided due to the fragile nature of platey and pumiceous glass shards; hence, no attempt was made to clean the glass surfaces with hydrogen peroxide (H_2O_2) or etch the shards with hydrofluoric acid (HF) to remove their thin outer layer influenced by external alpha-dose rates. Contamination by non-glassy phases was assessed using TL sensitivity response, and visually confirmed by light microscopy and Scanning Energy Dispersive-Scanning SEM (EDS-SEM) geochemical mapping of discs used in TL analysis and by examination of preliminary N/50 Gy dose response curves (Fig. 6, S4; see Supplementary Information for details).

SAR-TL experiment

Based on findings from our preliminary experiments (Fig. 6; Supplementary Notes 2, 3), and after testing multiple aliquot methods [101], it was noted that the relatively high radiation doses needed to match natural signals from the early Quaternary Óþoli tephra analysis had potential to induce radiation colouring in the samples. Moreover, sensitivities in response to repeated 50 Gy irradiation and readout cycles tended to decline, suggesting that such radiation colouring was not being fully annealed by the TL heating cycle to 400 degrees. In recognition of this, to quantify equivalent doses and constrain ages for the Þórsmörk Ignimbrite and the Óþoli tephra, we adapted the Single-Aliquot Regeneration OSL (SAR-OSL) technique [103, 104] for TL analysis (SAR-TL) . In the SAR method, the same disc is exposed to a series of laboratory radiation doses prior to preheating and readout, followed by a test dose (TD) measurement to assess laboratory induced sensitivity changes across the measurement cycle. The natural TL was measured from purified glass on each disc, and TL was then artificially regenerated beyond the naturally accumulated TL by applying a series of laboratory radiation doses to each disc.

Stainless steel discs were cleaned with acetone and Electolube SCO200D silicone grease then loaded with 4–6 mg of purified volcanic glass concentrated in the central area of each disc. Read-outs were undertaken using a Scottish Universities Environmental Research Centre (SUERC) TL Research Reader consisting of an Electron Tubes 9883 QB Photo-multiplier Tube (PMT) fitted with Schott 7/59 and KG1 filters and continuously flushed with nitrogen to prevent oxidising reactions that might create spurious TL. Measurements were undertaken manually with real time analysis to monitor glow shapes, assess integrated photon count rates to define successive regeneration doses levels required, and check for signal quality. Discs were heated from room temperature to 400 °C at 5 °C s^{-1}. Blanks and blank

contamination discs were cleaned with acetone and sprayed with Electolube SCO200D silicone grease, were placed on the work surface and read out at the end of each session. Discs for the N/50 Gy and SAR-TL experiment were irradiated using a shielded ELSEC 9022 irradiator fitted with a 1.85 GBq ^{90}Sr β-ray source with a source to sample distance of 15 mm and a silicate dose rate of 3.353 ± 0.015 Gy min^{-1} for the N/50 Gy experiment and 3.270 ± 0.015 Gy min^{-1} for the later SAR-TL experiments. Reconstructing the large natural signal retained in the Óþoli tephra proved particularly time consuming due to its large stored natural dose. For this experiment a higher dose rate irradiator incorporating a 11.1 GBq ^{90}Sr β-ray source at a working distance of 7.5 mmm was used, yielding a mean dose rate in the central areas of the sample of 32.0 ± 0.6 Gy min^{-1} Both irradiators had been calibrated to high precision relative to the UK air kerma standards at the National Physical Laboratory (NPL) when commissioned in 1997, before this study.

SAR-TL Palaeodose reconstruction (D_e)

After the natural TL signal had been thermally removed and measured (read-out), the TL and test dose and read-out measurement cycle for each disc consisted of: (1) Individual disc irradiation (ÞIG: 50, 75, 100, 125, 150, 200, 300 Gy; ÓT: 500, 1000, 1500, 2000, 3000, 4000, 5000, 6000 Gy); (2) A short, high temperature (within-chamber) pre-heat of 220 °C for two minutes and 0–400 °C TL read-out; (3) Test-dose (TD), pre-heat, as stage 2, and 0–400 °C TL read-out. Disc-specific changes in sensitivity were in stage 3 were corrected by applying a test-dose (TD) after each successive regeneration dose (ÞIG = 25 Gy; ÓT = 100 Gy). Palaeodose (D_e) values for the Þórsmörk Ignimbrite ÞIG7 and the Óþoli tephra SUTL551 samples were calculated from standard error weighted regression of 200–400 °C, 10 °C integrated data (Tables 1, 2, S2, S4). The final weighted mean palaeodose values used in age estimates were

374 calculated from the most thermally stable peak intensity regions of the glow curve,
375 determined by a D_e plateau plot. In summary, D_e values were integrated over three
376 temperature regions that correspond to the wide (280–360 °C), median (290–330 °C) and
377 narrow (290-310 °C) TL intensity peak region of the glow curves (Figs. 7–8; Tables 1, 2).
378 Uncorrected (UC) and test-dose (sensitivity) corrected (TDC) regeneration curves, were
379 modelled using best mathematical fit (highest adjusted r^2 values, *p*-value <0.05) linear
380 regression (y=ax+b) and non-linear least squares saturating exponential regression analysis
381 ($y=a[1-e^{(-bx)}]$) applied to 10 °C interval datasets for both samples (Tables S2, S4). The non-
382 linear and non-saturating response of the Óþoli Tephra was also modelled using saturating
383 exponential + linear regression analysis ($y=a[1-e^{(-bx)}] + cx$) [following 66]. Regression results
384 shown in Tables 1 and 2 represent methods with the highest r^2 and lowest RMSE values (see
385 also Table S2, S4). Other regression models (e.g., saturating exponential, 2nd and 4th order
386 polynomial) were investigated (e.g., Table S4). Regression and statistical analysis was
387 undertaken in SigmaPlot (Systat Software Inc., San Jose California USA,
388 www.systatsoftware.com), XLSTAT (version 2010.3.09, www.xlstat.com).
389
390 Fading tests were conducted at the end of the measurement cycle using multiple aliquot
391 grouped approaches as suggested by Sanderson 1988 [116]. For this, two groups of discs were
392 defined for each sample. As these had same prior radiation and TL readout histories as each
393 other, both groups were expected to be in the same state, in respect of sensitivity and
394 sensitisation behaviour. One of the groups was irradiated to a 50 Gy dose, at the start of the
395 test period, and the other irradiated at the end of it – 5 x 10^6 seconds. Both were preheated
396 together, and then readout, in their 9th readout cycle since the start of the experiment. These
397 results were normalised to those obtained from a prompt readout in their 8th cycle. By double

398 normalising the data sets and comparing the results from the two groups, the fading quotient
399 associated with the dark storage for the period between prompt and stored readings was
400 obtained. This approach provides for replication across many discs, and importantly is not
401 affected by sensitivity changes in the samples (based on sensitisation between successive
402 irradiation and readout cycles), or in the equipment (since the readout sessions for both
403 groups of samples are conducted together both for the prompt and stored measurements).
404 The fading observed crosses log time cycles 4-5 and 6-7.
405
406 A similar approach was adopted by Ward [67], who studied TL dose response, from 200 Gy to
407 160 kGy, and stability of highly reproducible mass produced and fully melted silicate glass
408 slices (i.e., microscope cover slips). Fading tests using high dose (44 kGy) covered 11
409 logarithmically spaced post-irradiation intervals from 45 minutes after irradiation up to 35
410 days. After an initial rapid fading over the first few hours following irradiation, subsequent
411 losses diminished in rate as seen on a logarithmic time scale and appeared to be dominated
412 by thermal fading processes. On this basis, the procedure adopted in the study aimed to avoid
413 the immediate post-irradiation period. It is recognised that fading rates over longer
414 Quaternary timescales represent an extrapolation over any observable laboratory storage
415 test. Therefore, the results of the study were also be assessed relative to independent age
416 controls of the Óþoli tephra and ÞIG in this study.
417
418 ***Dose rate reconstruction (D_T)***
419 The overall dose rate to the tephra shards includes internally generated alpha and beta
420 contributions, and externally delivered alpha, beta, gamma components from the bulk
421 sediment matrix, which are attenuated by water, plus an external cosmic dose rate

component (Tables 3, 4). Bulk sample geochemical data, obtained by X-ray fluorescence (XRF) and Inductively Coupled Plasma-Mass Spectrometry (ICP-MS) analysis, was used to assess 'external' or 'bulk' matrix dose-rates. Bulk dose rate calculations were based on the infinite matrix assumption [100], which states that samples are essentially homogeneous on a macroscale. Shard-specific electron probe microanalysis (EPMA) potassium (K) data and ICP-MS analysis of the purified glass fraction U, Th and Rb data were used for (internal) glass-shard dose rate calculations, ($D_T^{shard}{}_{(in\text{-}situ\text{–}sat)}$) in Table 4, following [98, 100]. See Supplementary Note 1 for experimental procedures. We also compared dose rates derived from bulk and glass shard geochemistry with data derived from spectrometry measurements (Tables 3, 4, S5).

For the most realistic assessment of dose rate, we partitioned the shard alpha dose into an internal contribution, which is not subject to water-content attenuation, and an external alpha contribution, delivered across the pore space of the bulk matrix, which is attenuated by pore-water. For the final weighted mean glass-bulk dose rate model, $D_T^{glass–bulk}{}_{(in\text{-}situ\text{–}sat)}$ (Table 4), we partitioned the dose rate into internal glass shard and external matrix components according to water content attenuation as follows. Samples for this study were collected during the warmest and driest parts of the year. Since the Icelandic climate is significantly colder and wetter outside our sampling months of June-August, we defined the mean water content as the mid-point of the collected and saturated water content and applied a 15% error to cover possible fluctuations in water content during burial [following 105].

Dry dose rates were attenuated by appropriate factors before calculation of final 'wet' dose rates using equations in [100], as follows: α-wet = α-dry / (1 + 1.5WF); β-wet = β-dry / (1 +

1.25WF); γ-wet = γ-dry / (1 + 1.14WF), where W and F are as defined W = (saturation wet weight - dry weight) / (dry weight). F = average fractional water content during burial history and was determined for two scenarios: as received water content (*in-situ*) and average palaeowater content, i.e., the mid-point between *in-situ* and saturated water content, with error limits that encompass the measured $F_{in\text{-}situ}$ and $W_{saturation}$ values. Errors in $F_{in\text{-}situ}$ are mean ± 1σ of three representative measurements, while $W_{saturation}$ errors are measurement errors from six duplicate measurements.

Internal (glass) and external (bulk) dose rates were based on geochemical and/or spectrometry data according to the following equations: $D\alpha_T = k[\phi_g D\alpha_g + (1\text{-}\phi_M)WFD\alpha_M]$ and $D_{\beta T} = \phi_g D_\beta + (1\text{-}\phi_M)WFD_{\beta M}]$, where: ϕ_g, ϕ_M are published absorbed dose factors and $(1\text{-}\phi_M)$ attenuation factors [107–109] that correspond to the median grain size for glass shards and matrix, respectively. Spectrometry-based dose rates were calculated from *in-situ* portable gamma-spectrometry, thick source beta counting (TSBC) and alpha spectrometry measurements (see Supplementary Note 4 for experimental details). Geochemical-based dose rates were calculated from bulk and shard-specific geochemical data in Tables 4 and S1 using well-established conversion factors [109]. No thoron or radon loss was assumed in conversion calculations because samples are believed to be sufficiently compact. External attenuation factors for U, Th and K taken from [108] were based on a median grain-size of 100 μm. Equilibrium between U and Th decay was assumed as similarities between elemental and TSBC dose rates suggested that disequilibrium between decay products is minimal (Supplementary Note 4).

Results

Sample collection, purification & preliminary dose response screening

We collected light-tight TL samples from 17 out of 23 locations visited in the Þórsmörk region (Figs. 2, 3). Samples covered a wide range of rhyolitic material, including pumice, airfall ash layers dominated by glass shards, inter-bedded rhyolitic ash layers associated with pyroclastic flow deposits, and reworked ash deposits overlying the pumiceous rich horizons (Fig. 3; Table S1). Sampled pumice clasts were unwelded and typically c. 10–50 cm in diameter (Fig. 3m). Ten light-tight samples were collected from airfall and reworked Óþoli tephra deposits (Fig. 5). Light-tight samples of A1875 tephra were collected from three locations: 0.5 km SE of Víti within the caldera (ASK 5) (ash-rich layers C & D [90]), 55 km to the ENE of Víti at Fiskidalur (ASK 10), and 74 km NNE of Víti at Arnórsstaðamuli (ASK 11), where visible layers, up to 1 cm thick exist (Fig. 4). Ö1362 tephra samples were collected from three sites at 9 km (Kvísker), 65 km (Hólmur), 86 km (Fóssdalur) to the East of the volcano along the principal eruption plume axis (Fig. 4). The major element geochemical composition of the rhyolitic glass-shards in the Ö1362 tephra is most similar to those of the Þórsmörk Ignimbrite (Fig. S1).

Visual inspection under the microscope revealed the rhyolitic ash and pumice Þórsmörk Ignimbrite samples were >95% glass, and the Óþoli tephra samples were >99% clear, platey glass shards of rhyolitic composition (Fig. 6). The bulk A1875 and Ö1362 samples were composed of >90–95% platey or pumiceous volcanic glass shards (Fig. 6). Þórsmörk Ignimbrite samples had the highest glass-shard alkali (Na+K) content of samples examined (Fig. S1). No purified fractions or SEM-EDS geochemical maps of discs used in SAR-TL experiments had exceptionally high K, Na, Ca, indicative of possible feldspar contamination (K, Na, Ca)$AlSi_3O_8$,) (Fig. S5).

Using the purified 90-150 micron volcanic glass shard fraction of the four deposits, we thermally read out the natural signal and examined their response to a 50 Gy radiation dose. We also undertook TL bleaching, TL inducement and pre-heating tests (Figs. 6, S5; Supplementary Notes 2, 3). Results showed an age-related signal was retained by volcanic glass (Fig. 6), and that a fairly consistent volcanic glass-phase response to 50 Gy laboratory radiation dose existed across all samples. This was characterised by a broad peak intensity region of up to 10^3–10^4 counts per second (cps) between 200–400 °C (Fig. 6a-d, f). The natural TL signal retained by the A1875 and Ö1362 samples was too small for further quantitative analysis using the existing set up (Fig. 6). Bleaching and inducement tests showed the TL signal could not be fully removed by optical exposure and that a TL signal of similar magnitude to the natural Óþoli tephra signal could not induced by optical exposure. Manual pre-heats of 220 °C for two minutes, 155 °C for five hours or 135 °C for 16 hours all successfully removed the laboratory-induced low temperature (c. 110 °C) TL peak observed in the natural and 50 Gy dose response experiment (Figs. 6, S5; see Supplementary Note 2 for experimental details).

SAR-TL experiments & palaeodose reconstruction

The Þórsmörk Ignimbrite ÞIG 7 purified glass sample was significantly more sensitive (defined as TL intensity per unit applied dose) than the Óþoli Tephra sample and had a straightforward linear dose response in the 200–400 °C temperature region (Figs. 7a, 8a). Notably, SAR-TL regression curves used for final analysis of the ÞIG7 and the Óþoli Tephra samples had mean r^2 values consistently >0.98 with $p< 0.0001$ in the 240–360 °C peak intensity region (Tables 1, 2).

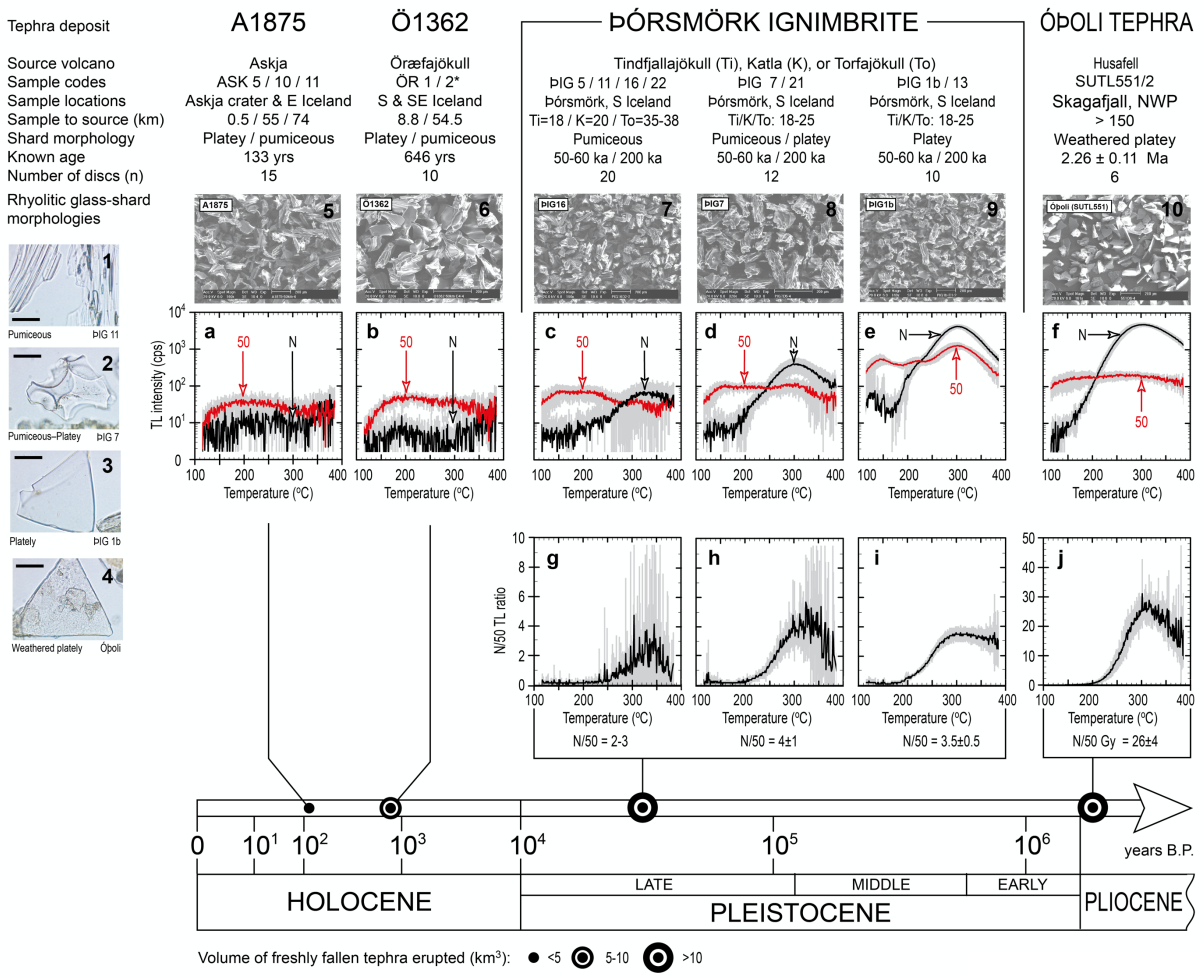

Figure 6. Preliminary natural versus 50 Gy (N/50 Gy) dose response tests for purified volcanic glass samples. (a)–(f) black lines represent the mean natural TL intensity (N) in counts per second (cps), at 1 °C intervals. Dark (red) lines represent the mean TL intensity produced by applying a 50 Gy laboratory dose. Light grey lines are ± 1σ errors from n discs shown at 1 °C intervals. Pre-heats were deliberately not applied prior to the N or 50 Gy TL read outs to allow examination of the natural and dose response glow curve shape. This creates a low temperature peak visible in some 50 Gy response profiles (*e.g.*, ÞIG 1b and ÞIG 13). As no pre-heats or regression analysis were undertaken, the information contained in this figure is not linked to age estimates obtained from the SAR-TL experiment. **(g)–(j)** Natural and 50 Gy ratio plateau plots, showing the mean ratio and single standard deviation of the N/50 Gy TL response; *=ÖR 3 was visibly contaminated by minerals unrelated to the eruption

event and is not included for clarity. Microphotographs 1–4, taken at x400 magnification, illustrate the difference between pumice and platey glass shard morphologies; black scale bar is 25 mm; purified samples were mounted in Canada Balsam. Scanning Electron Microscope (SEM) microphotographs 5–10 show selected Ö1362, A1875, ÞIG7 and ÓT purified glass shards on discs used in the preliminary N/50 Gy experiment. Discs were carbon coated for SEM-EDS geochemical mapping causing low image resolution.

For ÞIG7, the uncorrected natural TL lies within an approximately linear growth phase of the regeneration curve, enabling reliable D_e values to be obtained by interpolation (Fig. 7b). Neither the type of regression curve fitted or the temperature integral chosen (280–360 °C , 290–330 °C or 290–310 °C peak intensity regions of the glow curve) made a significant impact on the reconstructed D_e value (Figure 7, Table 1). The ÞIG7 290–310 °C peak intensity region had the most stable D_e plateau region with the lowest measurement errors (Fig. 7c) and was chosen for D_e analysis. Uncorrected weighted linear (LIN) regression applied to 290–310 °C data produced a D_e value of 169 ± 4 Gy, while weighted saturating exponential (SE) regression produced a D_e of 165 ± 4 Gy (Fig. 7b; Table 1).

There was an approximately linear increase in TL intensity for ÞIG7 25 Gy test-doses TD1–TD9 (Fig. 6a–b). The ÞIG7 test-dose sensitivity-corrected 290–330 °C peak intensity weighted mean D_e values were 221 ± 6 Gy (LIN) and 217 ± 5 Gy (SE) (Fig. 7e). Peak region (290–310 °C) D_e values were similar (227 ± 8 Gy (LIN); 225 ± 8 Gy (SE)). Athermal fading did not appear to be a significant for ÞIG7, with 96% of the signal retained in the 290–330 °C and 99% in the 290–310 °C stable peak temperature regions after 60-day storage (Tables 1, S3). Test-dose (sensitivity) and 60-day storage loss-corrected SAR-TL D_e values across the 280–360 °C region

range from 226 ± 7 Gy to 234 ± 11 Gy (Table 1). The most accurate assessment of the ÞIG7 palaeodose is considered to be the weighted mean sensitivity and 60-day storage-corrected SAR-TL D_e value of 230 ± 11 Gy, obtained by weighted linear regression from the 290–310 °C peak intensity temperature region (Table 1).

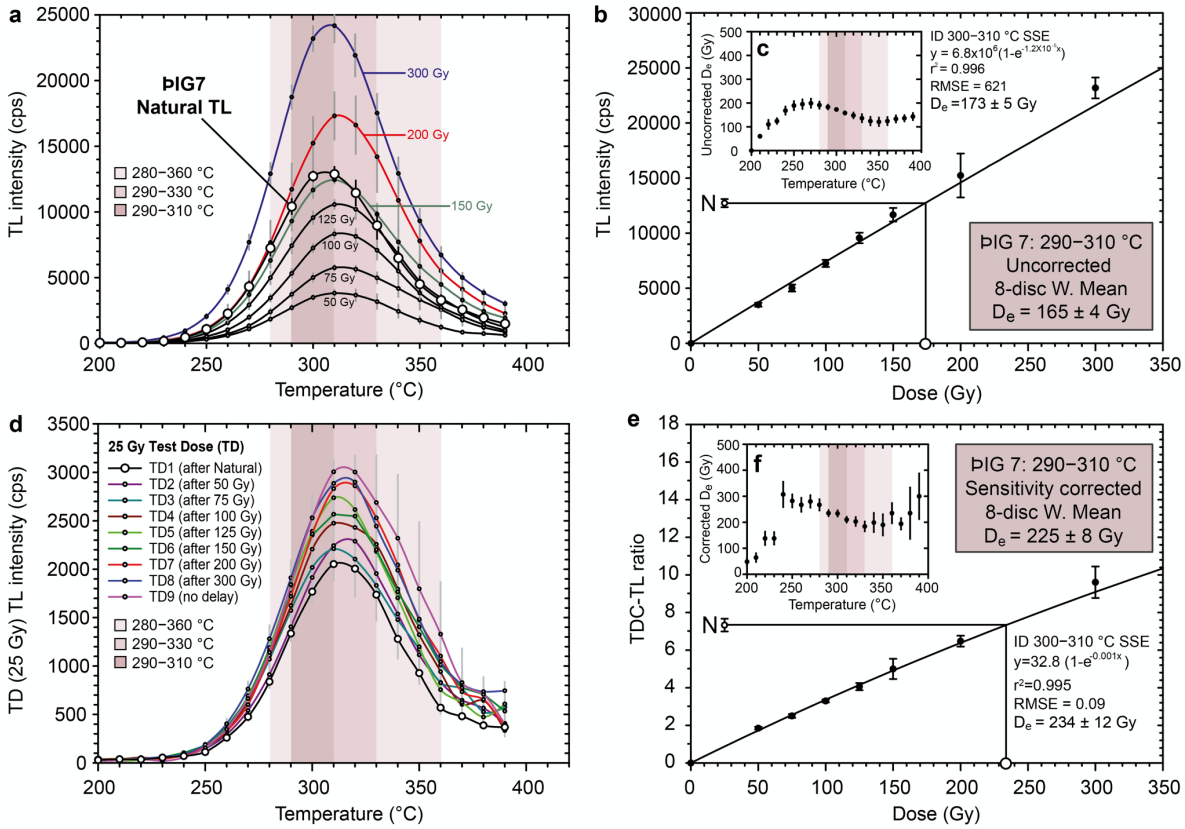

Figure 7. SAR-TL palaeodose (D_e) data for ÞIG 7 of the Þórsmörk Ignimbrite: (a) Natural and applied dose mean TL intensity glow curves. Weighted mean TL intensity standard measurement errors were 10.48 ± 1.32% in the 280–360 °C peak intensity region, 5.93 ± 0.66% for 290–330 °C and 5.95 ± 0.95% for 290–310 °C; **(b)** Example of a saturating exponential (SE) weighted regression curve fitting of the form $y=a[1-e^{(-bx)}]$ in the peak TL intensity 300-310 °C region. Similar SSE weighted regression was undertaken on 10-degree interval data between 200–400 °C to generate the D_e plateau plot shown in (c) (Tables 1, S2); **(c)** 200-400 °C D_e and temperature plateau plot; **(d)** 25 Gy test-dose (TD) mean TL intensity

567 glow curves; **(e)** Saturating exponential (SE) weighted regression of 300–310°C temperature
568 test-dose (sensitivity)-corrected data (see also Fig. S6); **(f)** 200–400 °C D_e temperature test-
569 dose (sensitivity) corrected D_e plateau plot. The weighted mean 290–310 °C sensitivity
570 corrected D_e = 225 ± 8 Gy. Results are based on 10 °C integration of original 1 °C data (Tables
571 1, S2).

Þórsmörk Ignimbrite Palaeodose Statistics & Age estimates					Weighted mean age (no fading correction)	60-day storage loss correction (Fraction of signal retained)	60-day storage loss corrected weighted mean palaeodose	60-day storage loss corrected weighted mean age	60-day storage loss corrected weighted mean age
ÞIG7 SAR-TL		Weighted mean palaeodose	8-Disc Mean Regression Error Analysis (all p<0.0001)						
		D_e ± SE (Gy)	Mean r^2 ± 1σ	Mean RMSE ± 1σ	$(D_T^{glass-bulk})_{(in-situ-sat)}$ 5.82 ± 1.48 (ka)		D_e ± SE (Gy)	$(D_T^{glass-bulk})_{(in-situ-sat)}$ 5.82 ± 1.48 mGy a^{-1} (ka)	$(D_T^{glass-bulk})_{(in-situ-sat)}$ 6.25 ± 1.51 mGy a^{-1} (ka)
Uncorrected	Linear regression								
	(a) 280-360 °C	157 ± 3	0.973 ± 0.025	639 ± 253	27 ± 7	**0.94 ± 0.04**	**167 ± 8**	**29 ± 7**	**27 ± 7**
	(b) 290-330 °C	166 ± 4	0.991 ± 0.009	527 ± 244	29 ± 7	**0.96 ± 0.02**	**173 ± 5**	**30 ± 8**	**28 ± 7**
	(c) 290-310 °C	169 ± 4	0.997 ± 0.003	352 ± 112	29 ± 7	**0.99 ± 0.03**	**171 ± 7**	**29 ± 8**	**27 ± 7**
	Saturating exponential regression								
	(d) 280-360 °C	151 ± 3	0.987 ± 0.009	511 ± 93	26 ± 7	**0.94 ± 0.04**	**160 ± 8**	**28 ± 7**	**26 ± 6**
	(e) 290-330 °C	158 ± 3	0.995 ± 0.003	543 ± 62	27 ± 7	**0.96 ± 0.02**	**165 ± 5**	**28 ± 7**	**26 ± 6**
	(f) 290-310 °C	165 ± 4	0.997 ± 0.003	528 ± 65	28 ± 7	**0.99 ± 0.03**	**167 ± 7**	**29 ± 7**	**27 ± 7**
Test dose-(Sensitivity-) corrected	Linear regression								
	(a) 280-360 °C	220 ± 5	0.984 ± 0.018	### ± 0.05	38 ± 10	**0.94 ± 0.04**	**234 ± 11**	**40 ± 10**	**37 ± 9**
	(b) 290-330 °C	221 ± 6	0.996 ± 0.004	### ± 0.03	38 ± 10	**0.96 ± 0.02**	**231 ± 8**	**40 ± 10**	**37 ± 9**
	(c) 290-310 °C	227 ± 8	0.999 ± 0.001	### ± 0.03	39 ± 10	**0.99 ± 0.03**	**230 ± 11**	**39 ± 10**	**37 ± 9**
	Saturating exponential regression								
	(d) 280-360 °C	215 ± 5	0.993 ± 0.009	### ± 0.06	37 ± 9	**0.94 ± 0.04**	**229 ± 11**	**39 ± 10**	**37 ± 9**
	(e) 290-330 °C	217 ± 5	0.999 ± 0.001	### ± 0.04	37 ± 10	**0.96 ± 0.02**	**226 ± 7**	**39 ± 10**	**36 ± 9**
	(f) 290-310 °C	225 ± 8	0.999 ± 0.001	### ± 0.05	39 ± 10	**0.99 ± 0.03**	**228 ± 10**	**39 ± 10**	**36 ± 9**

572

573 **Table 1. Summary palaeodose statistics and age estimates for the ÞIG7 sample.** The
574 weighted mean test-dose (sensitivity) and 60-day storage-loss corrected palaeodose and age
575 estimates shaded in dark grey and in bold are considered to be reliable. Best fit regression
576 analysis was determined from highest adjusted r^2 values. Ten-degree integrated ranges for
577 the 280–360 °C, 290–330 °C and 290–310 °C TL peak intensity regions are shown. The 290–
578 310 °C and 290–330 °C ranges (dark grey shading) have the lowest TL intensity measurement
579 errors, the highest 8-disc mean r^2, lowest RMSE values and lowest *p*-values. This produced
580 sensitivity and 60-day storage loss corrected palaeodoses of c. 230 ± 10 Gy and ages of 40 ±
581 10 ka. Data have been rounded to the nearest 10 Gy and 5 ka to reflect calculation errors,
582
583 In the 50 Gy dose response screening experiment, the natural TL signal from the Óþoli tephra
584 formed 'broad' unimodal peak of 10^3–10^4 cps $°C^{-1}$ between 280–360 °C (Fig. 6), indicating a

585 TL signal that is predominantly stored in the more stable, longer-term energy traps evicted at
586 high temperature. In the SAR-TL experiment, the uncorrected natural TL peak intensity region
587 of the glow curves from the Óþoli tephra (ÓT) covered a broader temperature range, 290–
588 330 °C, than ÞIG 7 (Fig. 8a). The broader shape of the regeneration dose response curve alone
589 implied that the ÓT was significantly older than the ÞIG7 sample (Fig. 8b). Regression results
590 show that the ÓT natural signal was located in an approximately linear growth phase *after* an
591 initial non-linear growth phase, best modelled by a saturating exponential plus linear
592 regression fit (Fig. 8b; Table S4). We chose this type of regression because it had a consistently
593 higher r^2 and lower RMSE values than single saturating exponential or polynomial (quadratic)
594 regression models (290-330 °C region mean $\pm$ 1σ r^2 = 0.995 $\pm$ 0.001; p<0.0001; Figs. 8b, S6;
595 Tables 2, S4). The 290–330 °C peak intensity region had the most stable D_e plateau, and
596 produced a weighted mean D_e value of 4581 $\pm$ 350 Gy (Fig. Table 2).
597
598 Assessing sensitivity change for the ÓT was more complex than for ÞIG7, with TL intensity
599 reversals between some adjacent 100 Gy test-dose runs (Fig. S6c–d). These non-linear effects
600 could be due to the (age-related) highly weathered and comparatively hydrated state of the
601 ÓT glass shards, the high laboratory dose rate, the higher magnitude of applied doses (>1
602 kGy), and/or cumulative radiation induced sensitivity changes (such as radiation 'colouring').
603 If the ÓT test-dose corrected response curve continued to grow in the same approximately
604 linear manner beyond 6 kGy, an applied dose in excess of 10 kGy would be required to
605 produce an interpolated sensitivity-corrected palaeodose estimate (Fig. 8e; Table 2). It was
606 not possible to apply such a high dose in the time available. Moreover, athermal fading
607 appeared to be a significant factor for the ÓT sample examined, with 73% the signal retained

608 in the 290–330 °C and 79% retained in the 290–310 °C stable peak temperature regions after
609 60-day storage (Tables 2, S3).

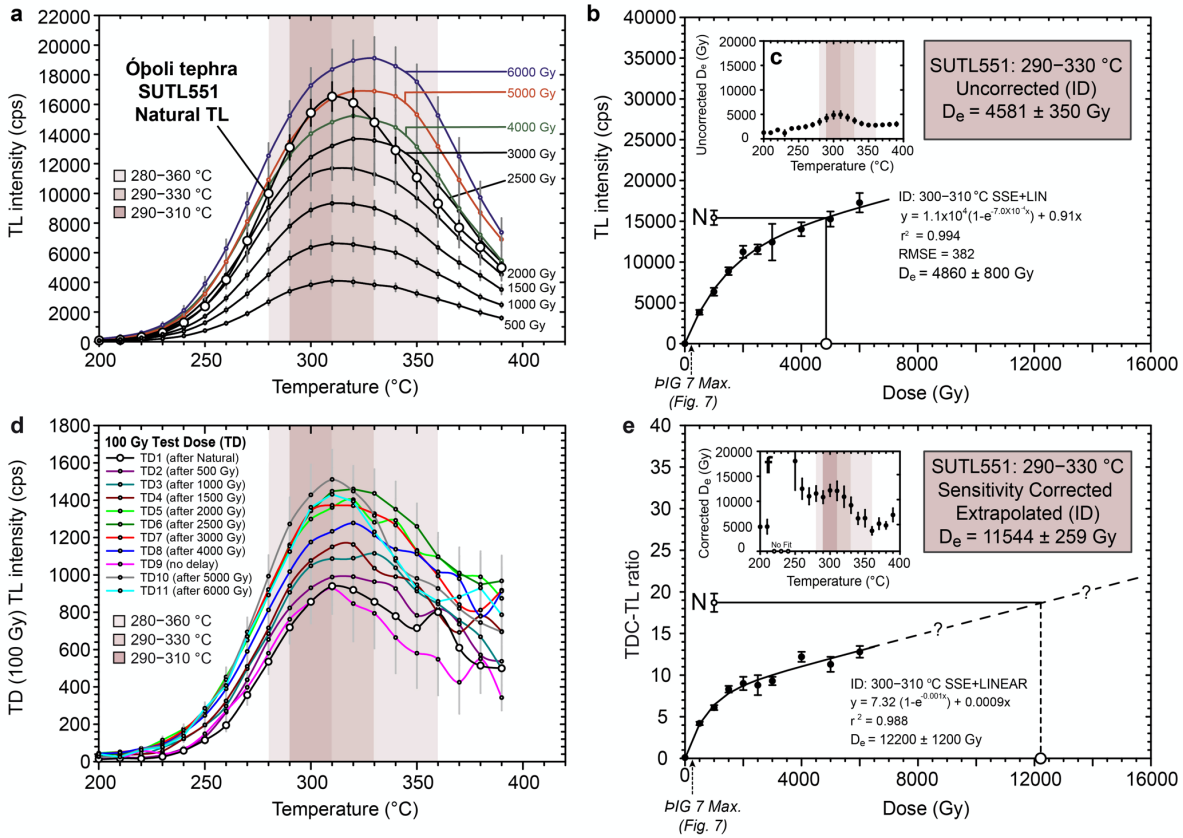

610

611 **Figure 8. SAR-TL D_e data for the Óþoli tephra airfall ash sample SUTL551***:* **(a)** Natural and
612 applied dose mean TL intensity glow curves. Weighted mean uncorrected TL intensity
613 measurement errors were 6.40 ± 0.11 % for the 280–360 °C peak intensity region, 6.37 ±
614 0.06% for 290–330 °C and 6.40 ± 0.13% for 290–310 °C; **(b)** Example of a saturating
615 exponential (SE) plus linear (LIN) weighted regression curve fitting $y = a[1-e^{(-bx)}]+cx$ in the peak
616 TL intensity 300–310 °C region. Similar SSE+LIN weighted regression was undertaken on 10
617 degree interval data between 200-400 °C to generate the D_e plateau plot shown in (c) (Tables
618 2, S4); **(c)** 200–400 °C D_e vs temperature plateau plot; **(d)** 100 Gy test-dose (TD) mean TL
619 intensity glow curves; **(e)** SE+LIN weighted regression of 300-310°C temperature peak region,
620 highlighting how the reconstructed natural test-dose (sensitivity) corrected is greater than

621 the highest applied dose of 6000 Gy (see also Fig. S6); **(f)** 200–400 °C (D_e) test-dose (sensitivity)
622 corrected palaeodose (D_e) plateau plot. Results shown are based on 10 °C integrals with
623 standard measurement error from measured 1 °C data (see also Tables 1, S3, S4).

Óþoli Tephra Palaeodose Statistics & Age estimates					Weighted mean age (no fading correction)	60-day storage loss correction (Fraction of signal retained)	60-day storage loss corrected weighted mean palaeodose	60-day storage loss corrected weighted mean age estimate	60-day storage loss corrected weighted mean age estimate
Óþoli Tephra (SUTL 551) SAR-TL		Weighted mean palaeodose	8-Disc Mean (8DM) Regression Error Analysis (all p<0.0001)						
		D_e ± SE (Gy)	Mean r^2 ± 1σ	Mean RMSE ± 1σ	$(D_T^{glass-bulk})_{(in-situ-sat)}$ 2.83 ± (ka)		D_e ± SE (Gy)	$(D_T^{glass-bulk})_{(in-situ-sat)}$ 3.97 ± 0.47 (ka)	$(D_T^{glass-bulk})_{(in-situ-sat)}$ 2.83 ± (ka)
Uncorrected	(a) 280-360 °C	3335 ± 155	0.995 ± 0.0015	331 ± 26	1178 ± 100	**0.74 ± 0.03**	**4505 ± 278**	**1135 ± 90**	**1592 ± 149**
	(b) 290-330 °C	4581 ± 350	0.995 ± 0.0012	342 ± 29	1619 ± 168	**0.73 ± 0.02**	**6294 ± 511**	**1585 ± 151**	**2224 ± 239**
	(c) 290-310 °C	4549 ± 524	0.995 ± 0.0002	355 ± 38	1607 ± 217	**0.79 ± 0.01**	**5764 ± 668**	**1452 ± 184**	**2037 ± 277**
Test-dose (Sensitivity) corrected	(a) 280-360 °C	8173 ± 153	0.986 ± 0.003	0.68 ± 0.13	2888 ± 211	**0.74 ± 0.03**	**11040 ± 493**	-	-
	(b) 290-330 °C	11544 ± 259	0.988 ± 0.003	0.58 ± 0.09	4079 ± 302	**0.73 ± 0.02**	**15861 ± 562**	-	-
	(c) 290-310 °C	11539 ± 302	0.986 ± 0.003	0.63 ± 0.09	4077 ± 307	**0.79 ± 0.01**	**14622 ± 426**	-	-

624

625 **Table 2. Summary palaeodose statistics and age estimates for the Óþoli tephra, sample.**
626 Ten-degree integrated intensity ranges for the three peak temperature plateau regions 280–
627 360 °C, 290–330 °C and 290–310 °C are shown. The weighted mean sensitivity and 60-day
628 storage loss-corrected palaeodose and age estimates highlighted in light grey overlap the
629 fission-track age of 2.26 ± 0.11 Ma [75].

630

631 ***Dose rates and age estimates***

632 Environmental dose rates for ÞIG7, ÞIG1b and Óþoli tephra samples shown in Tables 3, 4 and
633 S5 were produced using well-established equations and dose rate conversion factors. For
634 ÞIG7, the spectrometry-based dose rate of 5.82 ± 1.48 mGy a^{-1} and geochemistry-based dose
635 rate of 6.25 ± 1.51 mGy a^{-1} in combination with the sensitivity and 60-day storage loss-
636 corrected palaeodose values of c. 230 ± 10 Gy produced age estimate of 40 ± 10 ka. High
637 errors of c. 25% are mainly due to large uncertainties associated with estimating palaeowater
638 content fluctuations. Due to erratic changes in sensitivity and unresolved, but significant,
639 athermal signal losses, we cannot currently reconstruct a reliable SAR-TL age estimate for the
640 Óþoli tephra sample. Interestingly, though, the minimum uncorrected age shown in Table 2

is 1178 ± 100 ka or 1.18 ± 0.1 Ma, and the 60-day storage loss-corrected SAR-TL D_e value of 6294 ± 511 Gy and a geochemical dose-rate of 2.83 ± 0.41 mGy a^{-1} produces an age estimate of 2,224 ± 239 ka (2.22 ± 0.24 Ma) (Table 2), which is similar to the Óþoli tephra glass-shard fission-track age of 2.26 ± 0.11 Ma [75].

Geochemistry		Latitude	Longitude	Sampling	D_{cosmic} [1]	Elemental concentrations				
Tephra Lab. Code	Matrix	(°N)	(°W)	Depth (m)	dose rate (mGy a^{-1})	n	K or K_2O* (wt %)	U (ppm)	Th (ppm)	Rb (ppm)
Þórsmörk Ignimbrite										
ÞIG 7	Bulk	63°40.37	19°34.37	1 ± 0.5	0.16 ± 0.06	-	3.03 ± 0.15	3.80 ± 0.19	13 ± 0.7	107 ± 5
	Glass					20	4.07 ± 0.19*	4.37 ± 0.22	14.3 ± 0.7	-
ÞIG 1b	Bulk	63°40.35	19°36.22	20 ± 5	0.04 ± 0.01	-	3.28 ± 0.16	3.13 ± 0.16	10 ± 0.5	73 ± 4
	Glass					24	4.11 ± 0.61*	3.39 ± 0.17	11.6 ± 0.6	-
Óþoli Tephra										
SUTL551/2	Bulk	65°59.78	23°45.40	5 ± 1	0.11 ± 0.04	-	2.16 ± 0.11	2.26 ± 0.03	8.5 ± 0.4	55 ± 3
	Glass					137	2.75 ± 0.14*	2.60 ± 0.10	10.8 ± 0.5	-

Table 3. Location and geochemical data used to calculate dose rates for the Þórsmörk Ignimbrite and Óþoli tephra samples. [1]The cosmic dose rate calculation assumes no change in sediment depth throughout burial and was calculated from $0.21e^{[-0.07(dr)+0.0005(dr)^2]}$ mGy a^{-1} [following 130] where d is current depth of burial and r is the density of the attenuating medium where r = 0.998 g cm^{-3} for water and 2.6 g cm^{-3} were used for sediment; n = number of shards analysed (Supplementary Note 1 and Table S1 for details).

Dose rate data		**Glass shard dose rates**					**Bulk matrix dose rates**					**Weighted mean**
Tephra Lab ID	Measurement technique	$D\alpha_T$	$D\beta_T$	$D\gamma_T$	D_{cos}	$(D_T^{glass})_{(in\text{-}situ\ to\ sat)}$	$D\alpha_T$	$D\beta_T$	$D\gamma_T$	D_{cos}	$(D_T^{bulk})_{(in\text{-}situ\text{-}sat)}$	$(D_T^{glass\text{-}bulk})_{(in\text{-}situ\ to\ sat)}$
		(mGy a^{-1})				(mGy a^{-1})	(mGy a^{-1})				(mGy a^{-1})	(mGy a^{-1})
Þörsmórk Ignimbrite												
ÞIG 7	α-dose excluded	-	-	-	-	-	-	2.81	1.07	0.16	2.85 ± 0.60	2.85 ± 0.60
	Spectrometry*	1.84	2.12	1.09	0.16	5.22 ± 2.11	3.04	2.12	1.07	0.16	6.39 ± 2.07	**5.82 ± 1.48**
	Geochemical	1.84	2.09	1.09	0.16	5.18 ± 2.38	3.04	3.32	1.09	0.16	6.97 ± 1.96	**6.25 ± 1.51**
ÞIG 1b	α-dose excluded	-	-	-	-	-	-	2.55	1.09	0.05	2.96 ± 0.57	2.96 ± 0.57
	Spectrometry*	1.72	1.91	1.11	0.04	4.78 ± 2.12	2.43	1.91	1.09	0.05	5.48 ± 2.03	5.14 ± 1.47
	Geochemical	1.71	2.30	1.11	0.05	5.17 ± 2.64	2.43	3.12	1.11	0.05	6.71 ± 2.14	6.10 ± 1.66
Óþoli Tephra												
	α-dose excluded	-	-	-	-	-	-	1.59	0.56	0.11	1.83 ± 0.17	1.83 ± 0.17
	Spectrometry*	1.30	1.11	0.30	-	2.70 ± 0.62	1.51	1.11	0.30	-	2.92 ± 0.54	**2.83 ± 0.41**
	Geochemical	1.30	1.65	0.85	0.11	3.90 ± 0.66	1.51	1.58	0.85	0.11	4.04 ± 0.67	**3.97 ± 0.47**

Table 4. Summary dose rate data for the Þórsmörk Ignimbrite and Óþoli tephra samples. Summary dose rate values were calculated with α-dose rate excluded, using spectrometry data (α-dose included) and using geochemical data (α-dose included) for three scenarios:

glass shard, bulk matrix, and weighted mean (glass shard–bulk) matrix. Values in bold are considered most likely. For geochemical calculations, the glass shard matrix dose rate was calculated using well-established equations and conversion factors [107–109, 130–133]. Since the biggest source of uncertainty is variations in palaeowater content, using more recent conversion factors does not significantly alter these calculated dose rates or errors. Total alpha, beta and gamma dose rates ($D\alpha_T$, $D\beta_T$, $D\gamma_T$) incorporate attenuation factors based on *in situ*–saturation water content values [105, 132], which we consider to be most representative of the average water content through burial history at both the ÞIG 7 and Óþoli tephra sites (see Methods, Table S5). D_{cos} is the cosmic dose rate shown in Table 3. Errors for dose rate components are not shown for clarity but are typically $\pm$10%.

Discussion

We discuss the accuracy of the new ÞIG7 TL age estimate, examine implications of the age obtained, and make suggestions for future TL analysis of glass-rich tephra deposits based on the results from the ÞIG7 and Óþoli tephra experiments.

Experimental Implications

Our experiments on the Þórsmörk Ignimbrite (ÞIG7) produced age estimates that were similar orders of magnitude to published ages, highlighting that a glass-formation age-related TL signal is retained by the rhyolitic volcanic glass component of Icelandic tephra. In palaeodose reconstruction, even the smallest laboratory doses are applied at rates which are several orders of magnitude greater than those experienced in the natural environment. This creates two problems. First, high laboratory doses tend to fill or saturate shallow, thermally unstable traps, a process which does not occur during slower natural irradiation processes and may

680 result in differences in deep trap sensitivity [99, 110, 111]. Second, although laboratory dose
681 rates less than c. 10 Gy min^{-1} are not thought to be problematic [100], studies have shown
682 that laboratory irradiation at 10^8–10^{11} (c. 0.1–100 Gy min^{-1}) times greater than that
683 experienced in the natural environment can lead to defect creation, migration and,
684 ultimately, defect complex creation, which does not occur naturally [121]. Glass should be
685 one of the materials least affected, because localised charge transport is not favourable for
686 shallow-deep trap competition. The erratic sensitivity changes observed for the Óþoli tephra
687 in the SAR-TL experiment suggest the comparatively higher laboratory dose rates (an order
688 of magnitude greater than for the ÞIG7 sample) were detrimental in this respect. The obvious
689 solution is to reduce the applied dose rate, but this would be extremely time consuming for
690 multiple discs with several applied doses runs >1000 Gy.
691
692 Further investigation into the influence of sample age and applied dose on athermal signal
693 loss is recommended. This effect was minimal for the ÞIG sample but appears to be a
694 significant issue for the much older Óþoli tephra, which received applied doses in the c. 1-6
695 kGy range. From our investigations, the athermal signal loss characteristics of 'younger'
696 volcanic glass deposits appears to be similar to those of commercial glasses, which do not
697 exhibit significant athermal losses at 'low' applied doses i.e., <100 kGy [66]. Compositional
698 differences, additional lattice defects and/or weathering could explain the lower dose
699 threshold observed in our experiments.
700
701 Athermal fading of stored TL in phenocrysts of volcanic origin is thought to be responsible for
702 significant D_e underestimates in OSL dating of quartz phenocrysts present in some tephra
703 deposits from Japan [112, 114, 115] and infra-red stimulated luminescence (IRSL) dating of

volcanic feldspar and other phenocrysts in the Old Crow Tephra, Alaska [113]. 'Young' volcanic glass shards appear less susceptible to long-term athermal signal loss at low irradiation doses [65, 66, 110-115], perhaps because fewer opportunities for long-range charge transport exist in volcanic glass compared to mineral-based luminescence systems. The relatively small TL signals per unit dose and low short-range order of glasses may also result from increased opportunities for competing non-radiative relaxation. At low doses, recombination is most likely to take place in hole centres populated from non-correlated ionising events, leading to the type of reproducible dose response curves observed in the ÞIG7 sample. At higher doses (*e.g.*, >1 kGy) [66], the increased proximity between donors and acceptors pair may eventually favour tunnelling recombination and limit stability, as seen by the greater athermal losses in the Óþoli tephra.

By calculating the ionisation density as a function of dose, and partitioning the dose (energy per unit mass) amongst the atoms in feldspar, Sanderson [116] showed that the mean spacing of randomly positioned charge-carriers in a lattice irradiated at low doses was greater than 1000 lattice units. The random spatial model for fading in calcite [117], which has been subsequently applied to feldspars [116, 118], other minerals [119], and volcanic products [120] is perhaps less relevant for volcanic glass since it cannot support high rates of tunnelling at low dose without some form of charge-defect clustering, leading to deviations from the logarithmic (1/t) decay behaviour predicted by the Visocekas [117] model. Ward [66] showed that fading from glass cover slips across a range of doses up to 160 kGy exhibits logarithmic (1/t) decay behaviour only at the highest doses used. At very high doses, the proximity of neighbouring ion pairs becomes sufficiently close to enable anomalous signal losses from the glass matrix by quantum mechanical tunnelling [cf. 116], as observed by high dose

728 experiments from glass slices [66, 111]. In fact, all materials should exhibit (quantum
729 mechanical) tunnelling as the number of mean concentration of electron-ion pairs reaches
730 the percent level. If 1 kGy corresponds to 10 ppm initial ionisation, the mean concentration
731 of electron-ion pairs reaches the percent level at doses in the 10's-100's kGy region. At low
732 doses, thermal fading occurs from the continuum of traps where charge is located, and is
733 presumably lost to non-luminescence processes, but this is not necessarily a significant
734 barrier to successful dating providing the stability of the signal can be demonstrated by, for
735 example, the existence of stable thermal plateau plots.
736
737 In early work examining a range of glass-rich tephras Berger [73,74], expressed concern that
738 feldspar phenocrysts had potential to dominate fading behaviour for impure samples. He
739 noted the apparent stability of the glass rich tephra from the Mazama, tephra and suggested
740 that the glass phase experienced long-term athermal fading. Following the demonstration
741 that tephra showed weak OSL and IRSL response [75], Auclair [113] studied the potential of
742 IRSL dating from Crow Lake tephra from Alaska, in conjunction with stratigraphically
743 associated loess. The tephra samples, which had not been subject to flotation, had IRSL signals
744 which were an order of magnitude lower that the glass rich fractions, but, unlike samples used
745 in this study, retained plagioclase as well as volcanic glass, pyroxene and iron oxides. Three
746 approaches to fading analysis over a timescale ranging from 16 hours to 2000 hours were
747 examined, with differing results. When aliquots were irradiated and staggered intervals and
748 read together at the end of the storage period (to minimise the effects of sensitivity change
749 in readout equipment), scattered results were obtained, with a mean value of 2% fading per
750 decade of time. The use of short IRSL measurements, which scarcely depleted individual
751 aliquots, allowed multiple measurement from individual samples, and produced more

752 coherent data. Fading rates of 4% and 6% per decade were obtained from loess and tephra
753 samples, which are within uncertainties of each other. These values are very similar to values
754 obtained from feldspars. Auclair [113] noted the possibility that they may relate to the
755 phenocrysts in the sample, rather than the glass phase, and also noted the possible ambiguity
756 between fading and sensitivity change in the experimental design.
757
758 While our experiments suggest that the purification of coarser material from both PIG7 and
759 the Óþoli tephra was more successful, at this stage, it is not clear if storage signal losses
760 observed from the Óþoli tephra were due to insufficient thermal stability in the temperature
761 range examined, the onset of proximity effects or possibly related to the increased level of
762 weathering experienced by this sample over time. Despite low luminescence sensitivities, the
763 signal obtained from synthetic glasses continued to grow in a similar approximately linear
764 fashion after near-saturation to the Óþoli tephra [66]. This implies that dating of volcanic glass
765 up to at least two million years old could be possible, but several technical refinements are
766 needed to obtain accurate and reliable ages. Further high-dose experiments on volcanic glass
767 of Quaternary age and different geochemical composition are recommended to determine if
768 signal loss is related to burial age, geochemical composition and/or the scale of laboratory
769 doses or dose rates.
770
771 The other key factor in assessing the reliability of age estimates is the accuracy of calculated
772 dose rates. The large age errors in this study relate to the large dose rate errors and are
773 primarily due to long-term variations in palaeowater content during burial. However, our
774 dose rate calculations also had to account for variations in the alpha dose contribution since
775 it was not possible to etch the thin plately glass shards without destroying them. The alpha

776 dose contributed as much as 50% of the total dose rate in this study and creates uncertainties
777 that are as significant as those associated with changes in palaeowater content (Table 4). The
778 observed similarity between bulk and internal glass-shard compositions in both samples
779 examined suggests that sharp micro-dosimetric discontinuities probably do not exist at shard
780 boundaries. Nevertheless, whilst we constrained alpha dose-related uncertainties as far as
781 currently feasible, alpha dose attenuation in irregularly shaped glass shards could be
782 significantly different to published dosimetric equations, which are based on spherical grains
783 [100, 108, 122, 123]. Numerical modelling, beyond the scope of this paper, is therefore
784 recommended to fully evaluate the dosimetric properties of glass shard shapes that are not
785 perfect spheres. An in-depth comparison with dose rates from tephra deposits where volcanic
786 glass constitutes less than c. 95% of the bulk tephra matrix might also be useful.
787
788 In summary, we conclude that sensitivity and long-term storage tests are critical components
789 that should be included in all future analyses. Further reducing uncertainties associated with
790 our age estimates would also require extensive *in-situ* dose rate measurements, including for
791 example, a better assessment of seasonal to multi-decadal fluctuations in water content at
792 each site. Automation, single-grain glass shard analysis (where sensitivity allows) and pulsed-
793 laser infra-red stimulated luminescence (IRSL) methods could be applied and compared to
794 ages obtained from feldspar-phenocryst phases in glass-rich deposits. This could result in
795 reliable TL ages from tephra across a broad age-spectrum, up to and beyond the radiocarbon
796 dating upper limit of c. 50 ka.
797
798 ***Palaeoenvironmental Implications***

799 The c. 40 $\pm$ 10 ka age estimate of the ÞIG7 sample is similar in magnitude to existing age
800 estimates obtained from the Þórsmörk region. It is also a closer approximation to 'known'
801 ages for this deposit than, for example, the glass-phase TL age of 23.4 ± 2.4 ka obtained from
802 deposits associated with the c. 75 ka Toba eruption [124]. Post depositional thermal annealing
803 of the ÞIG7 sample could have reduced its measured age, but there are no currently active
804 thermal areas in the Þórsmörk valley. Our c. 40 $\pm$ 10 ka age estimate also eliminates the
805 possibility of a c. 200 ka eruption age for deposits at the ÞIG7 site. Following the SAR-TL
806 experiments, we examined glass shards in the ÞIG1b and ÞIG7 samples for the presence of
807 spontaneous fission-tracks. None were observed. The absence of natural fission-tracks in
808 volcanic glass with a c. 3–4.5 ppm uranium and c. 10-14.5 ppm thorium content provides an
809 additional age constraint of < c.100 ka, and rules out the possibility of a c. 200 ka eruption age
810 in more than one location within the Þórsmörk valley.
811
812 The 40±10 ka age is potentially younger than the established age of NAAZ2 and raises the
813 intriguing possibility of multiple ignimbrite- or rhyolitic-ash forming eruptions in the area
814 between 60-30 ka. Lacasse et al. [2, 4] first suggested the ÞIG is the terrestrial geochemical
815 equivalent of North Atlantic Ash Zone 2 (NAAZ-2). NAAZ-2 was originally dated in marine cores
816 to around 64 ka [46]. Later, correlation ages of 48.5-58 ka were proposed by comparing the
817 astronomically calibrated oxygen isotope time scale from marine cores with the Greenland
818 GISPII ice core incremental timescale [9, 86]. The widespread distribution of the Vedde Ash
819 and NAAZ-II in marine cores of the North Atlantic has been linked with ice rafting [9, 46],
820 raising doubts over the precision of c. 64-48 ka correlation ages for NAAZ-II in marine cores.
821 The spread of ages within NAAZ-II could also indicate more than one eruption event. Zielinski
822 et al. [9] proposed that NAAZ-II was the result of two simultaneous eruptions from Katla and

Torfajökull based on two distinct tephra deposits with similar chemical composition to NAAZ-II and the ÞIG found in Greenland ice cores at 53.5 ka and 57.3 ka [86, 87] (Fig. 9). The c. 40 ka age estimate for the ÞIG7 sample is approximately 23% younger these ice core ages, but coeval with an elevated volcanic sulphate peak in the GISP2 ice core record centred on 40 ka (Fig. 9). Moreover, the tephrochronology of 60-30 ka eruptions from Iceland has recently been geochemically mapped in unprecedented detail and supports the possibility of multiple large rhyolite-forming eruptions from volcanic complexes in and around Þórsmörk during this period.

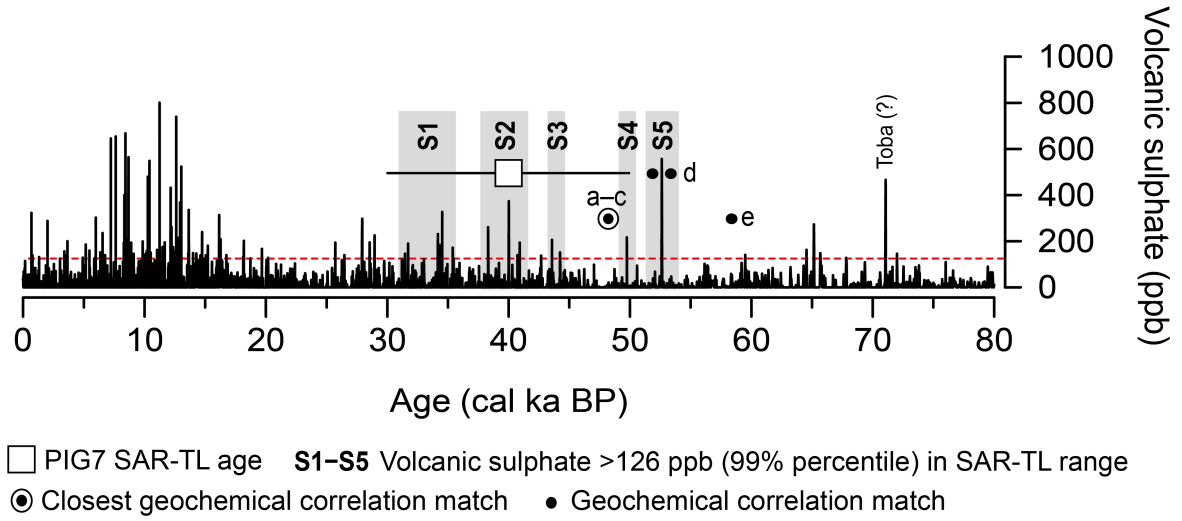

Figure 9 The GISP2 Volcanic Sulphate record of palaeovolcansim for the last 80,000 years compared to new SAR-TL age estimates for Þórsmörk Ignimbrite. Notes: IC ka = ice core years before present; References: (a) [53]; (b), (c) [2, 4]; (d) [9]; (e) [46].

To summarise, TL screening and dating of volcanic glass in tephra holds great potential, particularly for the rapid classification of geochemically similar volcanic systems with widely separated eruption events. Whether all the ignimbrite deposits in the Þórsmörk area are from the same eruption event remains uncertain and warrants further investigation. Luminescence

and radiometric dating of other deposits in the Þórsmörk area is recommended to determine if more than one ignimbrite-forming eruption event occurred between 60-30 ka and further improve the tephrochronological record of Iceland.

Conclusions

1) To improve the Late Pleistocene tephrochronology of Iceland, NW Europe, and the North Atlantic and Arctic regions, we investigated the thermoluminescence (TL) dose response characteristics of rhyolitic volcanic glass produced by four large Plinian eruptions from Iceland: the c. 50 ka Þórsmörk Ignimbrite, Askja 1875 AD, Öræfi 1362 AD and the Late Pliocene Óþoli Tephra,

2) Our screening experiments showed an unequivocal age-related increase in naturally retained glass-phase TL. Single aliquot regeneration-TL analysis of volcanic-glass from the Þórsmörk Ignimbrite produced an age estimate of c. 40 $\pm$ 10 ka, supporting evidence for a major eruption in the Þórsmörk area of Southern Iceland 30–60 ka rather than c. 200 ka.

3) The application of combined glass-phase thermoluminescence and radiometric dating at multiple sites in the Þórsmörk area could reveal if more than one ignimbrite-forming eruption occurred between 30-60 ka. Results from the Óþoli tephra were a similar order of magnitude to its established c. 2 Ma age, but further investigation of sensitivity change and signal loss from 'older' volcanic glass deposits is required. The tephrochronological record of Iceland could be improved using TL analysis of volcanic glass deposits.

Acknowledgements

SJR, AJD and DCWS undertook fieldwork funded by National Environmental Research Council (NERC) Grant no. GT 04/97/85/ES and the University of Edinburgh Moray Endowment Fund and Small Projects Grant; DCWS provided access to and support with luminescence analysis and interpretation. AJD acknowledges support of the National Science Foundation of America grant 1249313. SJR acknowledges additional support from BAS. The funders had no role in study design, data collection and analysis, decision to publish, or preparation of the manuscript. Thanks to Rob Austin-Smith, Tom Bradwell, Jeremy Everest and Bob McCulloch for their assistance in the field, John Westgate for examining Þórsmörk Ignimbrite ÞIG 1b and ÞIG7 samples for fission-tracks, Peter Hill, Paula McDade, Anthony Newton, and Shari Preece for assistance with geochemical analysis. The authors have no competing interests. Data availability: Datasets are summarised in the Supplementary Material and available from https://doi.org/10.6084/m9.figshare.13633877.v1, and the corresponding author (sjro@bas.ac.uk). All necessary permits were obtained for the described study, which complied with all relevant regulations.

References

1. Thórarinsson S. Ignimbrít í Þórsmörk. (Ignimbrite in Þórsmörk). Náttúrufræðingurinn. 1969;39:139-55.
2. Lacasse C, Sigurdsson H, Johannesson H, Paterne M, Carey S. Source of Ash-Zone-1 in the North-Atlantic. Bulletin of Volcanology. 1995;57(1):18-32. doi:10.1007/Bf00298704. PubMed PMID: WOS:A1995RB63400002.
3. Sigurdsson H, McIntosh WN, Dunbar N, Lacasse C, Carey SN. Thorsmörk ignimbrite in Iceland: possible source of North Atlantic Ash Zone 2. EOS Trans American Geophysical Union, Boston, 26-29 May 1998. 1998;EOS Trans. AGU, Spring Meet. Suppl.(79(17)):S172.
4. Lacasse C, Sigurdsson H, Carey S, Paterne M, Guichard F. North Atlantic deep-sea sedimentation of Late Quaternary tephra from the Iceland hotspot. Marine Geology. 1996;129(3-4):207-35. doi:10.1016/0025-3227(96)83346-9. PubMed PMID: WOS:A1996TV77400003.
5. Blockley SPE, Bourne AJ, Brauer A, Davies SM, Hardiman M, Harding PR, et al. Tephrochronology and the extended intimate (integration of ice-core, marine and terrestrial records) event stratigraphy 8–128 ka b2k. Quaternary Science Reviews. 2014;106:88-100. doi: http://dx.doi.org/10.1016/j.quascirev.2014.11.002.
6. Thórarinsson S. Askja on fire. Reykjavík: Almenna Bókafélagid; 1963.

7. Dugmore AJ. Tephrochronological studies of Holocene glacier fluctuations in south Iceland. In: Oerlemans J, editor. Glacier fluctuations and climatic change: Kluwer Academic Publishers; 1989. p. 37-55.
8. Zielinski GA, Germani MS, Larsen G, Baillie MGL, Whitlow S, Twickler MS, et al. Evidence of the Eldgja (Iceland) Eruption in the Gisp2 Greenland Ice Core - Relationship to Eruption Processes and Climatic Conditions in the 10th-Century. Holocene. 1995;5(2):129-40. doi:10.1177/095968369500500201. PubMed PMID: WOS:A1995RB22100001.
9. Zielinski GA, Mayewski PA, Meeker LD, Gronvold K, Germani MS, Whitlow S, et al. Volcanic aerosol records and tephrochronology of the Summit, Greenland, ice cores. Journal of Geophysical Research-Oceans. 1997;102(C12):26625-40. doi:10.1029/96jc03547. PubMed PMID: WOS:A1997YJ67100027.
10. Dugmore AJ, Newton AJ, Edwards KJ, Larsen G, Blackford JJ, Cook GT. Long-distance marker horizons from small-scale eruptions: British tephra deposits from the AD 1510 eruption of Hekla, Iceland. Journal of Quaternary Science. 1996;11(6):511-6. doi: 10.1002/(Sici)1099-1417(199611/12)11:6<511::Aid-Jqs284>3.0.Co;2-C. PubMed PMID: WOS:A1996WE01200006.
11. Larsen G, Dugmore A, Newton A. Geochemistry of historical-age silicic tephras in Iceland. Holocene. 1999;9(4):463-71. doi:10.1191/095968399669624108. PubMed PMID: WOS:000081526000007.
12. Wastegard S, Wohlfarth B, Subetto DA, Sapelko TV. Extending the known distribution of the Younger Dryas Vedde Ash into northwestern Russia. Journal of Quaternary Science. 2000;15(6):581-6. doi:10.1002/1099-1417(200009)15:6<581::Aid-Jqs558>3.3.Co;2-V. PubMed PMID: WOS:000089379900003.
13. Wastegard S, Turney CSM, Lowe JJ, Roberts SJ. New discoveries of the Vedde Ash in southern Sweden and Scotland. Boreas. 2000;29(1):72-8. PubMed PMID: WOS:000086023300006.
14. Wastegard S, Rasmussen TL. New tephra horizons from Oxygen Isotope Stage 5 in the North Atlantic: correlation potential for terrestrial, marine and ice-core archives. Quat Sci Rev. 2001;20(15):1587-93. doi:10.1016/S0277-3791(01)00055-5. PubMed PMID: WOS:000171249500002.
15. Wastegard S, Hall VA, Hannon GE, van den Bogaard C, Pilcher JR, Sigurgeirsson MA, et al. Rhyolitic tephra horizons in northwestern Europe and Iceland from the AD 700s-800s: a potential alternative for dating first human impact. Holocene. 2003;13(2):277-83. doi: 10.1191/0959683603hl617rr. PubMed PMID: WOS:000181279000011.
16. Wastegard S, Bjorck S, Greve C, Rasmussen TL. A tephra-based correlation between the Faroe Islands and the Norwegian Sea raises questions about chronological relationships during the last interglacial. Terra Nova. 2005;17(1):7-12. doi: 10.1111/j.1365-3121.2004.00578.x. PubMed PMID: WOS:000227350400002.
17. Wastegard S. Late Quaternary tephrochronology of Sweden: a review. Quaternary International. 2005;130:49-62. doi: 10.1016/j.quaint.2004.04.030. PubMed PMID: WOS:000226424200005.
18. Wastegard S, Rasmussen TL, Kuijpers A, Nielsen T, van Weering TCE. Composition and origin of ash zones from Marine Isotope Stages 3 and 2 in the North Atlantic. Quat Sci Rev. 2006;25(17-18):2409-19. doi: 10.1016/j.quascirev.2006.03.001. PubMed PMID: WOS:000240819000024.

19. Rasmussen TL, Wastegard S, Kuijpers E, van Weering TCE, Heinemeier J, Thomsen E. Stratigraphy and distribution of tephra layers in marine sediment cores from the Faeroe Islands, North Atlantic. Marine Geology. 2003;199(3-4):263-77. doi: 10.1016/S0025-3227(03)00219-6. PubMed PMID: WOS:000185176400004.
20. Wallrabe-Adams HJ, Lackschewitz KS. Chemical composition, distribution, and origin of silicic volcanic ash layers in the Greenland-Iceland-Norwegian Sea: explosive volcanism from 10 to 300 ka as recorded in deep-sea sediments. Marine Geology. 2003;193(3-4):273-93. doi: Pii S0025-3227(02)00661-8 Doi 10.1016/S0025-3227(02)00661-8. PubMed PMID: WOS:000181296600007.
21. Davies SM, Branch NP, Lowe J, Turney CSM. Towards a European tephrochronological framework for termination 1 and the early holocene. Philosophical Transactions of the Royal Society of London Series a-Mathematical Physical and Engineering Sciences. 2002;360(1793):767-802. doi: 10.1098/rsta.2001.0964. PubMed PMID: ISI:000175121800010.
22. Davies SM, Wastegard S, Wohlfarth B. Extending the limits of the Borrobol Tephra to Scandinavia and detection of new early Holocene tephras. Quaternary Research. 2003;59(3):345-52. doi: 10.1016/S0033-5894(03)00035-8. PubMed PMID: WOS:000183386500007.
23. Davies SM, Wastegard S, Rasmussen TL, Svensson A, Johnsen SJ, Steffensen JP, et al. Identification of the Fugloyarbanki tephra in the NGRIP ice core: a key tie-point for marine and ice-core sequences during the last glacial period. Journal of Quaternary Science. 2008;23(5):409-14. doi: 10.1002/jqs.1182. PubMed PMID: WOS:000257958100002.
24. Davies SM, Abbott PM, Pearce NJG, Wastegard S, Blockley SPE. Integrating the INTIMATE records using tephrochronology: rising to the challenge. Quat Sci Rev. 2012;36:11-27. doi: 10.1016/j.quascirev.2011.04.005. PubMed PMID: WOS:000301825900003.
25. Davies SM, Abbott PM, Meara RH, Pearce NJG, Austin WEN, Chapman MR, et al. A North Atlantic tephrostratigraphical framework for 130–60 ka b2k: new tephra discoveries, marine-based correlations, and future challenges. Quaternary Science Reviews. 2014;106:101-21. doi: http://dx.doi.org/10.1016/j.quascirev.2014.03.024.
26. Pyne-O'Donnell SDF. Three new distal tephras in sediments spanning the Last Glacial-Interglacial Transition in Scotland. Journal of Quaternary Science. 2007;22(6):559-70. doi: 10.1002/jqs.1066. PubMed PMID: WOS:000249439600001.
27. Pyne-O'Donnell SDF, Blockley SPE, Turney CSM, Lowe JJ. Distal volcanic ash layers in the Lateglacial Interstadial (GI-1): problems of stratigraphic discrimination. Quat Sci Rev. 2008;27(1-2):72-84. doi: 10.1016/j.quascirev.2007.02.019. PubMed PMID: WOS:000254196600007.
28. Beget JE, Keskinen MJ. Trace-element geochemistry of individual glass shards of the Old Crow tephra and the age of the Delta glaciation, central Alaska. Quaternary Research. 2003;60(1):63-9. doi: 10.1016/S0033-5894(03)00095-4. PubMed PMID: WOS:000184258400008.
29. Dugmore AJ, Larsen G, Newton AJ. 7 Tephra Isochrones in Scotland. Holocene. 1995;5(3):257-66. doi:10.1177/095968369500500301. PubMed PMID: WOS:A1995RW28900001.
30. Pearce NJG, Alloway BV, Westgate JA. Mid-Pleistocene silicic tephra beds in the Auckland region, New Zealand: Their correlation and origins based on the trace element

analyses of single glass shards. Quaternary International. 2008;178:16-43. doi: 10.1016/j.quaint.2006.09.005. PubMed PMID: WOS:000255304900005.
31. Pearce NJG, Denton JS, Perkins WT, Westgate JA, Alloway BV. Correlation and characterisation of individual glass shards from tephra deposits using trace element laser ablation ICP-MS analyses: current status and future potential. Journal of Quaternary Science. 2007;22(7):721-36. doi: 10.1002/jqs.1092. PubMed PMID: WOS:000250415800007.
32. Pearce NJG, Eastwood WJ, Westgate JA, Perkins WT. Trace-element composition of single glass shards in distal Minoan tephra from SW Turkey. J Geol Soc. 2002;159:545-56. doi:10.1144/0016-764901-129. PubMed PMID: WOS:000177855400007.
33. Pearce NJG, Westgate JA, Perkins WT, Preece SJ. The application of ICP-MS methods to tephrochronological problems. Applied Geochemistry. 2004;19(3):289-322. doi: 10.1016/S0883-2729(03)00153-7. PubMed PMID: WOS:000189101300003.
34. Bertrand S, Castiaux J, Juvigne E. Tephrostratigraphy of the late glacial and Holocene sediments of Puyehue Lake (Southern Volcanic Zone, Chile, 40 degrees S). Quaternary Research. 2008;70(3):343-57. doi: 10.1016/j.yqres.2008.06.001. PubMed PMID: WOS:000260841600001.
35. Cioni R, D'Oriano C, Bertagnini A. Fingerprinting ash deposits of small scale eruptions by their physical and textural features. Journal of Volcanology and Geothermal Research. 2008;177(1):277-87. doi: 10.1016/j.jvolgeores.2008.06.003. PubMed PMID: WOS:000260986600021.
36. Davies SM. Were there two Borrobol Tephras during the early Lateglacial period: implications for tephrochronology? Quat Sci Rev. 2004;23(5-6):581-9. doi: 10.1016/j.quascirev.2003.11.006. PubMed PMID: ISI:000220163100004.
37. Davies SM, Abbott PM, Meara RH, Pearce NJG, Austin WEN, Chapman MR, et al. A North Atlantic tephrostratigraphical framework for 130-60 ka b2k: new tephra discoveries, marine-based correlations, and future challenges. Quat Sci Rev. 2014;106:101-21. doi: 10.1016/j.quascirev.2014.03.024. PubMed PMID: WOS:000348010900008.
38. Hillenbrand CD, Moreton SG, Caburlotto A, Pudsey CJ, Lucchi RG, Smellie JL, et al. Volcanic time-markers for Marine Isotopic Stages 6 and 5 in Southern Ocean sediments and Antarctic ice cores: implications for tephra correlations between palaeoclimatic records. Quat Sci Rev. 2008;27(5-6):518-40. doi: 10.1016/j.quascirev.2007.11.009. PubMed PMID: WOS:000255351900007.
39. Knott JR, Sarna-Wojcicki AM, Montanez IP, Wan E. Differentiating the Bishop ash bed and related tephra layers by elemental-based similarity coefficients of volcanic glass shards using solution inductively coupled plasma-mass spectrometry (S-ICP-MS). Quaternary International. 2007;166:79-86. doi: 10.1016/j.quaint.2006.12.014. PubMed PMID: WOS:000247166400008.
40. Pollard AM, Blockley SPE, Lane CS. Some numerical considerations in the geochemical analysis of distal microtephra. Applied Geochemistry. 2006;21(10):1692-714. doi: 10.1016/j.apgeochem.2006.07.007. PubMed PMID: WOS:000241641000008.
41. Tamura I, Yamazaki H, Mizuno K. Characteristics for the recognition of Pliocene and early Pleistocene marker tephras in central Japan. Quaternary International. 2008;178:85-99. doi: 10.1016/j.quaint.2007.04.002. PubMed PMID: ISI:000255304900009.
42. Turney CSM, Blockley SPE, Lowe JJ, Wulf S, Branch NP, Mastrolorenzo G, et al. Geochemical characterization of Quaternary tephras from the Campanian Province,

Italy. Quaternary International. 2008;178:288-305. doi: 10.1016/j.quaint.2007.02.007. PubMed PMID: WOS:000255304900023.
43. Shane P, Martin SB, Smith VC, Beggs KF, Darragh MB, Cole JW, et al. Multiple rhyolite magmas and basalt injection in the 17.7 ka Rerewhakaaitu eruption episode from Tarawera volcanic complex, New Zealand. Journal of Volcanology and Geothermal Research. 2007;164(1-2):1-26. doi: 10.1016/j.jvolgeores.2007.04.003. PubMed PMID: WOS:000248766400001.
44. Shane P, Nairn IA, Martin SB, Smith VC. Compositional heterogeneity in tephra deposits resulting from the eruption of multiple magma bodies: Implications for tephrochronology. Quaternary International. 2008;178:44-53. doi: 10.1016/j.quaint.2006.11.014. PubMed PMID: WOS:000255304900006.
45. Ruddiman WF, Glover LK. Ice-Rafted Volcanic Ash - a Tracer of North-Atlantic Paleo-Circulation. Transactions-American Geophysical Union. 1972;53(4):423-&. PubMed PMID: WOS:A1972L950100407.
46. Ruddiman WF, Glover LK. Vertical Mixing of Ice-Rafted Volcanic Ash in North-Atlantic Sediments. Geological Society of America Bulletin. 1972;83(9):2817-&. doi: Doi 10.1130/0016-7606(1972)83[2817:Vmoiva]2.0.Co;2. PubMed PMID: WOS:A1972N400300019.
47. Pollard AM, Blockley SPE, Ward KR. Chemical alteration of tephra in the depositional environment: theoretical stability modelling. Journal of Quaternary Science. 2003;18(5):385-94. doi: 10.1002/jqs.760. PubMed PMID: WOS:000184038700002.
48. Blockley SPE, Pyne-O'Donnell SDF, Lowe JJ, Matthews IP, Stone A, Pollard AM, et al. A new and less destructive laboratory procedure for the physical separation of distal glass tephra shards from sediments. Quat Sci Rev. 2005;24(16-17):1952-60. doi: 10.1016/j.quascirev.2004.12.008. PubMed PMID: WOS:000231044100015.
49. Casely AF, Dugmore AJ. Climate change and 'anomalous' glacier fluctuations: the southwest outlets of Myrdalsjokull, Iceland. Boreas. 2004;33(2):108-22. doi: 10.1080/03009480410001136. PubMed PMID: WOS:000221110900002.
50. Dugmore AJ, Church MJ, Mairs KA, McGovern TH, Perdikaris S, Vesteinsson O. Abandoned farms, volcanic impacts, and woodland management: Revisiting pjorsardalur, the "Pompeii of iceland". Arctic Anthropology. 2007;44(1):1-11. PubMed PMID: WOS:000248704400001.
51. Dugmore AJ, Sugden DE. Do the anomalous fluctuations of Solheimajökull reflect ice-divide migration. Boreas. 1991;20:105-13.
52. Edwards KJ, Dugmore AJ, Blackford JJ. Vegetational response to tephra deposition and land-use change in Iceland: a modern analogue and multiple working hypothesis approach to tephropalynology. Polar Record. 2004;40(213):113-20. doi:10.1017/S0032247403003000. PubMed PMID: WOS:000226634700003.
53. Haflidason H, Eiriksson J, Van Kreveld S. The tephrochronology of Iceland and the North Atlantic region during the Middle and Late Quaternary: a review. Journal of Quaternary Science. 2000;15(1):3-22. PubMed PMID: ISI:000085226600002.
54. Hallsdottir M. Pollen analytical studies of human influence on vegetation in relation to the Landnám tephra layer in southwest Iceland1987. 45 p.
55. Kirkbride MP, Dugmore AJ. Timing and significance of mid-Holocene glacier advances in northern and central Iceland. Journal of Quaternary Science. 2001;16(2):145-53. doi:10.1002/jqs.589. PubMed PMID: WOS:000167761700005.

56. Kirkbride MP, Dugmore AJ. Glaciological response to distal tephra fallout from the 1947 eruption of Hekla, south Iceland. Journal of Glaciology. 2003;49(166):420-8. doi:10.3189/172756503781830575. PubMed PMID: WOS:000220521200011.
57. Kirkbride MP, Dugmore AJ. Responses of mountain lee caps in central Iceland to Holocene climate change. Quat Sci Rev. 2006;25(13-14):1692-707. doi: 10.1016/j.quascirev.2005.12.004. PubMed PMID: WOS:000239940000019.
58. Larsen G, editor Holocene volcanism in Iceland and tephrochronology as a tool in volcanology. Iceland 2000 – Modern Processes and Past Environments; 2000 April 27th-29th, 2000; Keele University, UK.
59. Lawson IT, Gathorne-Hardy FJ, Church MJ, Newton AJ, Edwards KJ, Dugmore AJ, et al. Environmental impacts of the Norse settlement: palaeoenvironmental data from Myvatnssveit, northern Iceland. Boreas. 2007;36(1):1-19. doi: 10.1080/0300948060082798. PubMed PMID: WOS:000244148600001.
60. Larsen C, Newton AJ, Dugmore AJ, Vilmundardottir EG. Geochemistry, dispersal, volumes and chronology of Holocene from the Katla volcanic silicic tephra layers system, Iceland. Journal of Quaternary Science. 2001;16(2):119-32. PubMed PMID: WOS:000167761700003.
61. Wastegard S. Early to middle Holocene silicic tephra horizons from the Katla volcanic system, Iceland: new results from the Faroe Islands. Journal of Quaternary Science. 2002;17(8):723-30. doi: 10.1002/jqs.724. PubMed PMID: WOS:000180149700001.
62. Selbekk RS, Tronnes RG. The 1362 AD Oraefajoull eruption, Iceland: Petrology and geochemistry of large-volume homogeneous rhyolite. Journal of Volcanology and Geothermal Research. 2007;160(1-2):42-58. doi: 10.1016/j.jvolgeores.2006.08.005. PubMed PMID: WOS:000244215100003.
63. Sarna-Wojcicki A. Tephrochronology. In: Stratton-Noller J, Sowers, J. M., Lettis, W. R., editor. Quaternary Geochronology: Methods and Applications2000.
64. Shane P. Tephrochronology: a new Zealand case study. Earth-Science Reviews. 2000;49(1-4):223-59. doi:10.1016/S0012-8252(99)00058-6. PubMed PMID: WOS:000086702100005.
65. Aitken M.J., 1985, Thermoluminescence Dating, Academic Press
66a. Sanderson D, Warren SE, Hunter JR, editors. The TL properties of archaeological glass. Proceedings of 3rd Specialist seminar on TL and ESR dating; 1983; PACT 9(II), 287-298, ISBN 87-550-0915-8, Strasbourg
66b. Sanderson D.C.W., 1982, The thermoluminescence of archaeological glass, MPhil Thesis, University of Bradford)
67. Ward S. The thermoluminescence of glass slices and their potential as radiation dosimeters in the 0-160 kGy range.BSc dissertation, University of Strathclyde; 1988.
68. Huntley DJ, Bailey DC. Obsidian Source indetification by thermoluminescence. Archaeometry. 1978;20(2):159-70.
69. Westgate JA. Isothermal Plateau Fission-Track Ages of Hydrated Glass Shards from Silicic Tephra Beds. Earth and Planetary Science Letters. 1989;95(3-4):226-34. doi:10.1016/0012-821x(89)90099-X. PubMed PMID: WOS:A1989CC77700004.
70. Westgate J, Sandhu A, Shane P. Fission-Track Dating. In: Taylor RE, Aitken MJ, editors. Chronometric Dating in Archaeology. Boston, MA: Springer US; 1997. p. 127-58.
71. Westgate JA, Preece SJ, Froese DG, Walter RC, Sandhu AS, Schweger CE. Dating early and middle (Reid) pleistocene glaciations in central Yukon by tephrochronology.

Quaternary Research. 2001;56(3):335-48. doi:10.1006/qres.2001.2274. PubMed PMID: WOS:000172212000005.
72. Bigazzi G, Laurenzi MA, Soligo M, Tuccimei P. Multi-method approach to dating glass: The case of Basiluzzo Islet (Aeolian archipelago, Italy). Journal of Volcanology and Geothermal Research. 2008;177(1):244-50. doi: 10.1016/j.jvolgeores.2007.10.005. PubMed PMID: WOS:000260986600018.
73. Berger GW. The Use of Glass for Dating Volcanic Ash by Thermoluminescence. Journal of Geophysical Research-Solid Earth. 1991;96(B12):19705-20. doi: 10.1029/91jb01899. PubMed PMID: WOS:A1991GQ69100013.
74. Berger GW. Dating Volcanic Ash by Use of Thermoluminescence. Geology. 1992;20(1):11-4. doi:10.1130/0091-7613(1992)020<0011:Dvabuo>2.3.Co;2. PubMed PMID: WOS:A1992GZ53700003.
75 Roberts SJ, Sigurvinsson JR, Westgate JA, Sandhu A. Late Pliocene glaciation and landscape evolution of Vestfirðir, Northwest Iceland. Quat Sci Rev. 2007;26(1-2):243-63. doi: 10.1016/j.quascirev.2006.09.004. PubMed PMID: ISI:000244024800017.
76. Jorgensen KA. The Thorsmork Ignimbrite - an Unusual Comenditic Pyroclastic Flow in Southern Iceland. Journal of Volcanology and Geothermal Research. 1980;8(1):7-22. doi:10.1016/0377-0273(80)90004-9. PubMed PMID: WOS:A1980KF92900002.
77. Jorgensen KA. The eruption of Þórsmörk Ignimbrite, south Iceland. Reykjavik: Nordic Volcanological Institute, Report no. 8103., 1981.
78. McGarvie DW, editor Torfajökull – the world's most active rhyolite volcano. Iceland 2000 – Modern Processes and Past Environments; 2000 April 27th-29th 2000; Keele University, UK.
79. Thórarinsson S, Sæmundsson K. Volcanic activity in historical time. Jökull. 1979;29:29-32.
80. Jakobsson SP. Outline of the petrology of Iceland. Jökull. 1979;29:57-73.
81. Jakobsson SP. Chemistry and distribution pattern of Recent basaltic rocks in Iceland. Lithos. 1972;5:365-86.
82. Imsland P. The Petrology of Iceland: Some General Remarks. Reykjavik: Nordic Volcanological Institute Report 7808, pp. 2, 1978.
83. Sæmundsson K. Outline of the Geology of Iceland. Jökull. 1979;29:7-28.
84. Jorgensen KA. Mineralogy and Petrology of Alkaline Granophyric Xenoliths from the Thorsmork Ignimbrite, Southern Iceland. Lithos. 1987;20(2):153-68. doi: Doi 10.1016/0024-4937(87)90004-1. PubMed PMID: WOS:A1987G439900004.
85. Sparks RSJ, Bursik MI, Carey SN, Gilbert JS, Glaze LS, Sigurdsson H, et al. Volcanic Plumes. Chichester: John Wiley and Sons; 1997. 574 p.
86. Ram M, Gayley RI. Long-Range Transport of Volcanic Ash to the Greenland Ice-Sheet. Nature. 1991;349(6308):401-4. doi:10.1038/349401a0. PubMed PMID: WOS:A1991EV51400045.
87. Ram M, Donarummo J, Sheridan M. Volcanic ash from Icelandic similar to 57,300 yr BP eruption found in GISP2 (Greenland) ice core. Geophysical Research Letters. 1996;23(22):3167-9. doi:10.1029/96gl03099. PubMed PMID: WOS:A1996VQ92400025.
88. Haflidason H, Eiriksson J, Van Kreveld S. The tephrochronology of Iceland and the North Atlantic region during the Middle and Late Quaternary: a review. Journal of Quaternary Science. 2000;15(1):3-22. PubMed PMID: ISI:000085226600002.

89. Sparks RSJ, Wilson L, Sigurdsson H. The Pyroclastic Deposits of the 1875 Eruption of Askja, Iceland. Philos T R Soc A. 1981;299(1447):241-+. doi:10.1098/rsta.1981.0023. PubMed PMID: WOS:A1981LA47100001.
90. Sigurdsson H, Sparks RSJ. Petrology of Rhyolitic and Mixed Magma Ejecta from the 1875 Eruption of Askja, Iceland. Journal of Petrology. 1981;22(1):41-84. PubMed PMID: WOS:A1981LD62800002.
91. Macdonald R, Sparks RSJ, Sigurdsson H, Mattey DP, Mcgarvie DW, Smith RL. The 1875 Eruption of Askja Volcano, Iceland - Combined Fractional Crystallization and Selective Contamination in the Generation of Rhyolitic Magma. Mineralogical Magazine. 1987;51(360):183-202. doi:10.1180/minmag.1987.051.360.01. PubMed PMID: WOS:A1987H622300001.
92. Mohn H. Askeregnen den 29de-30te Marts 1875. Forhandlinger i Videnskaps-selskabet i Christiania aar 1877. 1877;10: 1–12.
93. Einarsson T. Tephrochronology. In: Berglund BE, editor. Handbook of Holocene Palaeoecology and Palaeohydrology: John Wiley and Sons; 1986. p. 329-42.
94. Bergman J, Wastegard S, Hammarlund D, Wohlfarth B, Roberts SJ. Holocene tephra horizons at Klocka Bog, west-central Sweden: aspects of reproducibility in subarctic peat deposits. Journal of Quaternary Science. 2004;19(3):241-9. doi: 10.1002/jqs.833. PubMed PMID: WOS:000221238800003.
95. Pilcher JR, Hall VA, Mccormac FG. Dates of Holocene Icelandic Volcanic-Eruptions from Tephra Layers in Irish Peats. Holocene. 1995;5(1):103-10. doi:10.1177/095968369500500111. PubMed PMID: WOS:A1995QX87900011.
96. Thórarinsson S. The Öræfajökull eruption of 1362. Acta Naturalia Islandica. 1958;2(2):1-99.
97. Sigurvinsson JR. Weichselian glacial lake deposits in the Highlands of north-western Iceland. Jökull. 1983;33:99-109.
98. McKeever SWS. Thermoluminescence of solids. Cambridge: Cambridge University Press; 1985. 312 p.
99. Wintle AG. Luminescence dating: Laboratory procedures and protocols. Radiation Measurements. 1997;27(5-6):769-817. doi:10.1016/S1350-4487(97)00220-5. PubMed PMID: WOS:000072413000007.
100. Aitken MJ. An introduction to optical dating. The Dating of Quaternary Sediments by the Use of Photon-stimulated Luminescence. Oxford: Oxford University Press; 1998. 270 p.
101. Zander A, Duller GAT, Wintle AG. Multiple and single aliquot luminescence dating techniques applied to quartz extracted from Middle and Upper Weichselian loess, Zemechy, Czech Republic. Journal of Quaternary Science. 2000;15(1):51-60. doi:10.1002/(Sici)1099-1417(200001)15:1<51::Aid-Jqs468>3.0.Co;2-6. PubMed PMID: WOS:000085226600005.
102. Turney CSM, Harkness DD, Lowe JJ. The use of microtephra horizons to correlate Late-glacial lake sediment successions in Scotland. Journal of Quaternary Science. 1997;12(6):525-31.doi:10.1002/(Sici)1099-1417(199711/12)12:6<525::Aid-Jqs347>3.3.Co;2-D. PubMed PMID: WOS:000071733500007.
103. Murray AS, Wintle AG. Luminescence dating of quartz using an improved single-aliquot regenerative-dose protocol. Radiation Measurements. 2000;32(1):57-73. doi: 10.1016/S1350-4487(99)00253-X. PubMed PMID: WOS:000084790600008.

104. Murray AS, Wintle AG. The single aliquot regenerative dose protocol: potential for improvements in reliability. Radiation Measurements. 2003;37(4-5):377-81. doi: 10.1016/S1350-4487(03)00053-2. PubMed PMID: WOS:000184110400015.
105. Pawley SM, Bailey RM, Rose J, Moorlock BSP, Hamblin RJO, Booth SJ, et al. Age limits on Middle Pleistocene glacial sediments from OSL dating, north Norfolk, UK. Quat Sci Rev. 2008;27(13-14):1363-77. doi: 10.1016/j.quascirev.2008.02.013. PubMed PMID: WOS:000257604000006.
106. Zimmerman DW. Thermoluminescent Dating Using Fine Grains from Pottery. Archaeometry. 1971;13(Feb):29-52. doi: DOI 10.1111/j.1475-4754.1971.tb00028.x. PubMed PMID: WOS:A1971Y040400005.
107. Bell WT. Alpha dose attenuation in quartz grains for thermoluminescence dating. Ancient TL. 1980;12:4-8.
108. Mejdahl V. Thermoluminescence Dating - Beta-Dose Attenuation in Quartz Grains. Archaeometry. 1979;21(Feb):61-72. doi: DOI 10.1111/j.1475-4754.1979.tb00241.x. PubMed PMID: WOS:A1979GM02300005.
109. Nambi KSV, Aitken MJ. Annual Dose Conversion Factors for TL-and-ESR Dating. Archaeometry. 1986;28:202-5. doi10.1111/j.1475-4754.1986.tb00388.x. PubMed PMID: WOS:A1986D630100007.
110. Wintle AG. Detailed Study of a Thermoluminescent Mineral Exhibiting Anomalous Fading. Journal of Luminescence. 1977;15(4):385-93. doi:10.1016/0022-2313(77)90037-0. PubMed PMID: WOS:A1977EB75500002.
111. Sanderson DCW. Thermoluminescence dating of Scottish vitrified forts: Paisley College of Technology; 1986 uk.bl.ethos.376105
112. Toyoda S, Tsukamoto S, Hameaua S, Usui H, Suzuki T. Dating of Japanese Quaternary tephras by ESR and luminescence methods. Quaternary Geochronology. 2006;1(4):320-6. doi: 10.1016/j.quageo.2006.03.007. PubMed PMID: WOS:000247209900010.
113. Auclair M, Lamothe M, Lagroix F, Banerjee SK. Luminescence investigation of loess and tephra from halfway house section, central Alaska. Quaternary Geochronology. 2007;2(1-4):34-8. doi: 10.1016/j.quageo.2006.05.009. PubMed PMID: WOS:000247210000008.
114. Tsukamoto S, Murray AS, Huot S, Watanuki T, Denby PM, Botter-Jensen L. Luminescence property of volcanic quartz and the use of red isothermal TL for dating tephras. Radiation Measurements. 2007;42(2):190-7. doi: 10.1016/j.radmeas.2006.07.008. PubMed PMID: WOS:000247516300010.

115. Tsukamoto S. Luminescence, Volcanic Rocks. In: Rink JW, Thompson J, editors. Encyclopedia of Scientific Dating Methods. Dordrecht: Springer Netherlands; 2013. p. 1-5.
116. Sanderson DCW. Fading of Thermo-Luminescence in Feldspars - Characteristics and Corrections. Nuclear Tracks and Radiation Measurements. 1988;14(1-2):155-61. PubMed PMID: WOS:A1988P853300023.
117. Visocekas R. La luminescence de la calcite après irradiation cathodique: thermoluminescence et luminescence par effet tunnel. France: Université de Pierre et Marie Curie; 1979.
118. Lamothe M, Auclair M. A solution to anomalous fading and age shortfalls in optical dating of feldspar minerals. Earth and Planetary Science Letters. 1999;171(3):319-23. doi: 10.1016/S0012-821x(99)00180-6. PubMed PMID: WOS:000082374200001.

119. Templer RH. The Localised Transition Model of Anomalous Fading. 1986. p. 493-7.
120. Morthekai P, Jain M, Murray AS, Thomsen KJ, Botter-Jensen L. Fading characteristics of martian analogue materials and the applicability of a correction procedure. Radiation Measurements. 2008;43(2-6):672-8. doi: 10.1016/j.radmeas.2008.02.019. PubMed PMID: WOS:000257808000117.
121. Chawla S, Rao TKG, Singhvi AK. Quartz thermoluminescence: Dose and dose-rate effects and their implications. Radiation Measurements. 1998;29(1):53-63. doi: 10.1016/S1350-4487(97)00200-X. PubMed PMID: WOS:000072761500007.
122. Bell WT. Attenuation factors for the absorbed radiation dose in quartz grains for luminescence dating. Ancient TL. 1979;8:2-13.
123. Bell WT. TL dating: radiation dose rate data. Archaeometry. 1979;21:243.
124. Horn P, Müller-Sohnius D, Storzer D, Zöller L. K-Ar-, fission-track-, and thermoluminescence ages of Quaternary volcanic tuffs andtheir bearing on Acheulian artifacts from Bori,Kukdi Valley, Pune District, India. Zeitschriftder Deutschen geologischen Gesellschaft. 1993;144:326-9.
125. Wolfe CJ, Bjarnason IT, VanDecar JC, Solomon SC. Seismic structure of the Iceland mantle plume. Nature. 1997;385(6613):245-7. doi:10.1038/385245a0. PubMed PMID: WOS:A1997WC71100044.
126. LeMaitre RW, Bateman P, Dudek A, Keller J, Lameyre Le Bas MJ, Sabine PA, et al. A classification of igneous rocks and glossary of terms. Oxford: Blackwell; 1989.
127. Rickwood PC. Boundary Lines within Petrologic Diagrams Which Use Oxides of Major and Minor Elements. Lithos. 1989;22(4):247-63. doi:10.1016/0024-4937(89)90028-5. PubMed PMID: WOS:A1989U514400001.
128. Oskarsson N, Steinthorsson S, Sigvaldason GE. Iceland Geochemical Anomaly - Origin, Volcanotectonics, Chemical Fractionation and Isotope Evolution of the Crust. J Geophys Res-Solid. 1985;90(Nb12):11-25. doi:10.1029/JB090iB12p10011. PubMed PMID: WOS:A1985ASE4800005.
129. Sweatman TR, Long JVP. Quantitative electron microprobe analysis of rock forming minerals. Journal of Petrology. 1969;7:332-79.
130. Prescott JR, Hutton JT. Cosmic ray contributions to dose rates for luminescence and ESR dating: large depths and long-term time variations. Radiation Measurements. 1994;23(497-500).
131. Norrish K, Hutton JT. An accurate X-ray spectrographic method for the analysis of a wide range of geological samples. Geochimica et Cosmochimica Acta. 1969;33:431-53.
132. Aitken MJ, Bowman SGE. Thermoluminescence dating: assessment of alpha particle contribution. Archaeometry. 1975;17:132-8.
133. Berger GW. Progress in luminescence dating methods for Quaternary sediments. In: Rutter NW, Catto NR, editors. Dating Methods for Quaternary Deposits: Geological Association of Canada; 1995. p. 81-104.